NASA TN D-340

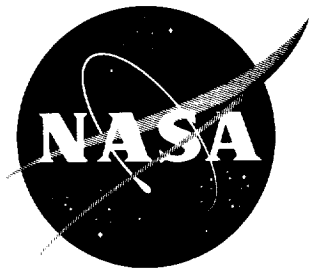

TECHNICAL NOTE

D-340

THE NUMERICAL CALCULATION OF FLOW PAST CONICAL BODIES SUPPORTING ELLIPTIC CONICAL SHOCK WAVES AT FINITE ANGLES OF INCIDENCE

By Benjamin R. Briggs

Ames Research Center
Moffett Field, Calif.

NATIONAL AERONAUTICS AND SPACE ADMINISTRATION

WASHINGTON November 1960

NATIONAL AERONAUTICS AND SPACE ADMINISTRATION

TECHNICAL NOTE D-340

THE NUMERICAL CALCULATION OF FLOW PAST CONICAL BODIES SUPPORTING ELLIPTIC CONICAL SHOCK WAVES AT FINITE ANGLES OF INCIDENCE

By Benjamin R. Briggs

SUMMARY

The inverse method, with the shock wave prescribed to be an elliptic cone at a finite angle of incidence, is applied to calculate numerically the supersonic perfect-gas flow past conical bodies not having axial symmetry. Two formulations of the problem are employed, one using a pair of stream functions and the other involving entropy and components of velocity. A number of solutions are presented, illustrating the numerical methods employed, and showing the effects of moderate variation of the initial parameters.

INTRODUCTION

The first three-dimensional high-speed flow problem to be solved exactly was the flow past a circular cone. Pioneers in this work were Busemann, and Taylor and Macoll. (See refs. 1 to 3.) Reference 4 gives numerical solutions for circular cones using the theory developed in reference 2. A perturbation technique was devised by Stone, reference 5, for circular cones at small angles of yaw. The method of Stone was applied in reference 6 to obtain approximate solutions for cones at small angles of yaw, and was extended in reference 7 for large angles of yaw. A somewhat similar numerical analysis, the linear characteristics method, was developed by Ferri for analyzing the flow past yawed circular cones (ref. 8) and slightly noncircular cones (refs. 9 and 10). Tables, based on the method of Ferri, are available (ref. 11) for calculating such flows. Of the various analyses referred to above, the only exact numerical solutions, based on the full inviscid equations of motion, are the ones tabulated in reference 4. They were obtained by numerical integration of the equations of motion specialized for symmetrical conical flow.

There are various ways that an exact (numerical) attack on a high-speed flow problem, employing the full inviscid equations of motion, might be organized. One is to specify conditions at the body and then to integrate the equations of motion outwardly toward the shock wave.

This is the manner in which the problem was posed for the integrations tabulated in reference 4. Another way is to prescribe conditions at the shock wave and then to integrate inwardly toward the body. This has been called the "inverse" or "marching inward" method. The capabilities of this method are exemplified in the work of Van Dyke and Gordon, reference 12, who presented a catalog of solutions of flows past blunt bodies for a large family of preassigned shock shapes. In the work of Radhakrishnan, reference 13, the marching inward technique was used to find the conical body behind a circular conical shock wave at a large angle of yaw. In reference 14, Briggs employed an analogous approach to compute bodies that support elliptic conical shocks.

The work of reference 14 is extended here to include circular or elliptic conical shock waves at finite angles of attack or yaw. Two implementations of the inverse method are employed, and each has been programmed for an electronic computer. The first formulation, which was used in reference 14, is in terms of pressure, density, and a pair of stream functions, one of which vanishes at the body. (A discussion of the use of several stream functions in the analysis of three-dimensional flows will be found in reference 15.) The second formulation of the problem is in terms of velocity components, pressure, density, and entropy. The body is located by calculating the position of the entropy layer, shown by Ferri (ref. 8) to exist on the surface of the body in the case of nonsymmetrical conical flow. The computations of reference 13 were based on this latter approach. (An interesting discussion relative to the thickness of the aforementioned entropy layer is given by Cheng, ref. 16.)

The flow field behind an elliptic conical shock wave is analyzed in detail in the present report, both the stream-function and velocity-entropy formulations of the problem being used. The resulting body and surface pressure is given, along with plots of the variation of the velocity components and entropy in the flow field. A diagram showing the stream lines in the crossflow is also presented. Comparisons are shown between results of wind-tunnel tests on elliptic cones and numerical calculations with initial data based on schlieren pictures of the shock waves in these tests. A comparison with the approximate theory of reference 6 is made using a machine result calculated with a circular conical shock wave at a finite angle of yaw. Finally, the results of a number of cases are presented wherein systematic variations of shock geometry, free-stream Mach number, and ratio of specific heats were made. These are given in the form of body shape and surface pressure.

SYMBOLS

a_1, b_1 semimajor and semiminor axes of elliptic cross section of coordinate surface of constant $\theta = \theta_0$ (eqs. (4))

a_2, b_2	semimajor and semiminor axes of elliptic cross section of coordinate surface of constant $\varphi = \varphi_o$ (eqs. (4))
A, B, C, D	functions defined by equations (8)
f, g	stream functions of a three-dimensional flow
F, G	specializations of f and g for the present conical flow problem
h_1, h_2, h_3	coefficients of the metric of the sphero-conal coordinate system
k^2, k'^2	constants in the sphero-conal coordinate transformation
M	Mach number
n	number of points taken in the numerical integration
N	function defined by equation (41)
p	pressure referred to $\rho_\infty U_\infty^2$
r, θ, φ	sphero-conal coordinates (see fig. 2)
S	entropy, $\frac{p}{\rho^\gamma}$
u, v, w	velocity components in the sphero-conal coordinates
u_1, v_1, w_1	velocity components in Cartesian coordinates
U_∞	free-stream velocity
$\vec{V}$	velocity vector
x, y, z	Cartesian coordinates
γ	ratio of specific heats
$\Gamma(x, y, z)$	coordinate surface that coincides with the shock wave
$\Delta\theta, \Delta\varphi$	increments of θ and φ that define the mesh size in the numerical calculations
ρ	density referred to free-stream value

Subscripts

b	conditions on the body surface
n	nth extrapolation
N	normal component (eq. (23))
O	conditions at the shock wave
r,θ,φ	differentiation with respect to variables r,θ,φ
x,y,z	differentiation with respect to variables x,y,z
∞	free-stream conditions

Superscripts

(n)	nth extrapolation
'	differentiation with respect to the variable G

THE SPHERO-CONAL COORDINATE SYSTEM

The numerical procedure employed here requires that the shock wave be a coordinate surface. A system of orthogonal coordinates r,θ,φ which meets this requirement is given in reference 17. The transformation from Cartesian coordinates is

$$\left.\begin{aligned} x &= r\cos\theta\sqrt{1-k'^2\cos^2\varphi} \\ y &= r\sin\theta\sin\varphi \\ z &= r\cos\varphi\sqrt{1-k^2\cos^2\theta} \\ k^2 + k'^2 &= 1\ , \qquad 0 \le \theta \le \pi\ , \qquad 0 \le \varphi \le 2\pi \end{aligned}\right\} \tag{1}$$

where x,y,z are the Cartesian coordinates. The element of length in the sphero-conal coordinates system is defined by the relation

$$ds^2 = h_1^2dr^2 + h_2^2d\theta^2 + h_3^2d\varphi^2 \tag{2}$$

where

$$\left.\begin{aligned} h_1^2 &= 1 \\ h_2^2 &= r^2 \frac{k^2\sin^2\theta + k'^2\sin^2\varphi}{1-k^2\cos^2\theta} \\ h_3^2 &= r^2 \frac{k^2\sin^2\theta + k'^2\sin^2\varphi}{1-k'^2\cos^2\varphi} \end{aligned}\right\} \qquad (3)$$

The coordinate surfaces are:

$$\left.\begin{aligned} x^2 + y^2 + z^2 &= r^2 \quad \text{for fixed} \quad r = r_o \\ x^2 - \frac{y^2}{b_1^2} - \frac{z^2}{a_1^2} &= 0 \quad \text{for fixed} \quad \theta = \theta_o \\ \frac{x^2}{a_2^2} + \frac{y^2}{b_2^2} - z^2 &= 0 \quad \text{for fixed} \quad \varphi = \varphi_o \\ a_1^2 &= \frac{1-k^2\cos^2\theta_o}{k^2\cos^2\theta_o} \\ b_1^2 &= \tan^2\theta_o \qquad a_1 \geq b_1 \\ a_2^2 &= \frac{1-k'^2\cos^2\varphi_o}{k'^2\cos^2\varphi_o} \\ b_2^2 &= \tan^2\varphi_o \qquad a_2 = \geq b_2 \end{aligned}\right\} \qquad (4)$$

Portions of the conical surfaces that are represented by the second and third of equations (4) are shown in figure 1. The shock wave of the present problem will be taken as a constant θ ($=\theta_o$) surface.

The components u, v, and w of velocity in the sphero-conal coordinate system are in the directions of increasing r, θ, and φ, respectively. Figure 2 shows curves of constant θ and φ as projected onto the y-z plane. The velocities v_1 and w_1 are in the directions of increasing y and z, respectively, and the velocity u_1, not shown in figure 2, is in the direction of increasing x.

The relationship between Cartesian and sphero-conal components of velocity is given by the equations:

$$\left.\begin{aligned}
u_1 &= u\cos\theta\sqrt{1-k'^2\cos^2\varphi} - v\sin\theta\sqrt{\frac{(1-k^2\cos^2\theta)(1-k'^2\cos^2\varphi)}{k^2\sin^2\theta + k'^2\sin^2\varphi}} \\
&\quad + w\frac{k'^2\sin\varphi\cos\varphi\cos\theta}{\sqrt{k^2\sin^2\theta + k'^2\sin^2\varphi}} \\
v_1 &= u\sin\theta\sin\varphi + v\cos\theta\sin\varphi\sqrt{\frac{1-k^2\cos^2\theta}{k^2\sin^2\theta + k'^2\sin^2\varphi}} \\
&\quad + w\sin\theta\sin\varphi\sqrt{\frac{1-k'^2\cos^2\varphi}{k^2\sin^2\theta + k'^2\sin^2\varphi}} \\
w_1 &= u\cos\varphi\sqrt{1-k^2\cos^2\theta} + v\frac{k^2\sin\theta\cos\theta\cos\varphi}{\sqrt{k^2\sin^2\theta + k'^2\sin^2\varphi}} \\
&\quad - w\sqrt{\frac{(1-k^2\cos^2\theta)(1-k'^2\cos^2\varphi)}{k^2\sin^2\theta + k'^2\sin^2\varphi}}
\end{aligned}\right\} \quad (5)$$

THE EQUATIONS OF MOTION

The equations of motion for flow of an ideal compressible fluid are, in vector form,

$$\operatorname{div}(\rho\vec{V}) = 0 \qquad \text{(continuity)} \qquad (6a)$$

$$\rho(\vec{V}.\operatorname{grad})\vec{V} + \operatorname{grad} p = 0 \qquad \text{(momentum)} \qquad (6b)$$

$$\vec{V}.\operatorname{grad}(p/\rho^\gamma) = 0 \qquad \text{(energy)} \qquad (6c)$$

The velocity $\vec{V}$ has been made dimensionless with respect to free-stream velocity U_∞, density ρ with respect to free-stream density ρ_∞, and pressure with respect to the quantity $\rho_\infty U_\infty^2$. When transformed into the sphero-conal system, equations (6) become

$$A\frac{\partial(\rho v)}{\partial\theta} + B\frac{\partial(\rho w)}{\partial\varphi} + \rho(2u+ACv+BDw) = 0 \qquad (7a)$$

$$Av\frac{\partial u}{\partial\theta} + Bw\frac{\partial u}{\partial\varphi} - (v^2+w^2) = 0 \qquad (7b)$$

$$Av\frac{\partial v}{\partial\theta} + Bw\frac{\partial v}{\partial\varphi} - ACw^2 + uv + BDvw + \frac{A}{\rho}\frac{\partial p}{\partial\theta} = 0 \qquad (7c)$$

$$Av\frac{\partial w}{\partial\theta} + Bw\frac{\partial w}{\partial\varphi} - BDv^2 + uw + ACvw + \frac{B}{\rho}\frac{\partial p}{\partial\varphi} = 0 \qquad (7d)$$

$$Av\frac{\partial(p/\rho^\gamma)}{\partial\theta} + Bw\frac{\partial(p/\rho^\gamma)}{\partial\varphi} = 0 \qquad (7e)$$

Note that the assumption of conical flow has been made in the writing of equations (7) and that the following abbreviations have been employed:

$$\left.\begin{aligned} A^2 &= \frac{1-k^2\cos^2\theta}{k^2\sin^2\theta + k'^2\sin^2\varphi} = \frac{r^2}{h_2^2} \\ B^2 &= \frac{1-k'^2\cos^2\varphi}{k^2\sin^2\theta + k'^2\sin^2\varphi} = \frac{r^2}{h_3^2} \\ C &= \frac{k^2\sin\theta\cos\theta}{k^2\sin^2\theta + k'^2\sin^2\varphi} \\ D &= \frac{k'^2\sin\varphi\cos\varphi}{k^2\sin^2\theta + k'^2\sin^2\varphi} \end{aligned}\right\} \qquad (8)$$

Three-dimensional flows such as those under discussion can be described by a method utilizing two functions which are a generalization of the familiar stream function of two-dimensional and axisymmetric flows. This technique was used in reference 14, and a concise description of the use of stream functions in the analysis of three-dimensional flow problems can be found in reference 15.

If two functions, f and g, are chosen such that

$$\rho\vec{V} = (\text{grad } f) \times (\text{grad } g) \qquad (9)$$

then equation (6a) is satisfied, and f and g represent stream surfaces whose intersections are streamlines. This can be demonstrated in the following manner.

Equation (9) has the three Cartesian components

$$\left.\begin{aligned} \rho u &= f_y g_z - f_z g_y \\ \rho v &= f_z g_x - f_x g_z \\ \rho w &= f_x g_y - f_y g_x \end{aligned}\right\} \qquad (10a)$$

where subscripts x,y,z indicate partial differentiation. From equations (10a) it follows that

$$u:v:w = (f_y g_z - f_z g_y):(f_z g_x - f_x g_z):(f_x g_y - f_y g_x) \qquad (10b)$$

Equation (10b) is a solution of the two equations

$$\left.\begin{aligned} \vec{V}\cdot\text{grad } f &= 0 \\ \vec{V}\cdot\text{grad } g &= 0 \end{aligned}\right\} \qquad (11)$$

Equations (11) are valid if $\vec{V}$, the velocity vector, is normal to grad f and grad g. Grad f and grad g are the normals to surfaces f and g, and so $\vec{V}$ must lie in the surfaces f and g. It can be said, then, that f and g surfaces contain the streamlines, and that the intersections of these surfaces are the streamlines. Thus it is quite reasonable to think of f and g as stream functions.

The energy equation, equation (6c), now takes the form

$$\frac{p}{\rho^{\gamma}} = S(f,g) \qquad (12)$$

which states that entropy is constant along streamlines. The momentum equation, equation (6b), can be written in terms of $\vec{V}$, ρ, and S; that is,

$$\rho(\vec{V}\cdot\text{grad})\vec{V} + \text{grad}[\rho^{\gamma} S(f,g)] = 0 \qquad (13)$$

The velocity components u,v,w can be found in terms of the stream functions f and g by expanding equation (9). The result, in the sphero-conal coordinate system, is

$$\left.\begin{aligned} u &= \frac{AB}{\rho r^2}\left(f_\theta g_\varphi - f_\varphi g_\theta\right) \\ v &= \frac{B}{\rho r}\left(f_\varphi g_r - f_r g_\varphi\right) \\ w &= \frac{A}{\rho r}\left(f_r g_\theta - f_\theta g_r\right) \end{aligned}\right\} \qquad (14)$$

Here f and g are functions of r,θ,φ and the subscripts indicate partial differentiation. Equations (14) are general for three-dimensional flows and are not limited to conical flows.

For conical flow $\vec{V}$, ρ, and S are not functions of r. Thus it is clear from equations (14) that the product fg is homogeneous of order 2 in r. In order that f will reduce to Stokes' stream function in the axisymmetric case and that the body be described by $f = 0$, it is convenient to make the definitions

$$\left.\begin{aligned} f(r,\theta,\varphi) &= r^2 F(\theta,\varphi) \\ g(r,\theta,\varphi) &= G(\theta,\varphi) \end{aligned}\right\} \qquad (15)$$

Now S cannot be independent of r unless it is also independent of f. It can be concluded, then that

$$S(f,g) = S(G) \qquad (16)$$

for conical flow.

Equations (14) may now be formally written in terms of F and G; that is,

$$\left.\begin{aligned} u &= \frac{AB}{\rho}\left(F_\theta G_\varphi - F_\varphi G_\theta\right) \\ v &= -\frac{2B}{\rho} F G_\varphi \\ w &= \frac{2A}{\rho} F G_\theta \end{aligned}\right\} \qquad (17)$$

The components of $\text{grad}[\rho^\gamma S(G)]$ are

$$\left.\begin{array}{l} 0 \\ \dfrac{A\rho^{\gamma}S}{r}\left(r\,\dfrac{\rho_\theta}{\rho}+\dfrac{S'}{S}\,G_\theta\right) \\ \dfrac{B\rho^{\gamma}S}{r}\left(r\,\dfrac{\rho_\varphi}{\rho}+\dfrac{S'}{S}\,G_\varphi\right) \end{array}\right\} \qquad (18)$$

in the r,θ,φ directions. The equations of motion in terms of F and G are:

θ momentum:

$$[\gamma\rho^{\gamma+1}S - (2BFG_\varphi)^2]\,\frac{\rho_\theta}{\rho}$$

$$= (2BF)^2(G_\theta G_{\varphi\varphi}-G_\varphi G_{\theta\varphi}) - (\rho^{\gamma+1}S)\left(\frac{S'}{S}\right)G_\theta + 2B^2FG_\varphi(F_\varphi G_\theta - F_\theta G_\varphi)$$

$$+ (2F)^2G_\theta\left(D-B^2\,\frac{\rho_\varphi}{\rho}\right)G_\varphi + (2F)^2(B^2G_\varphi{}^2 + A^2G_\theta{}^2) \qquad (19)$$

φ momentum:

$$(2AF)^2G_\varphi G_{\theta\theta} = 2A^2FG_\theta(F_\varphi G_\theta - F_\theta G_\varphi) + (2AFG_\theta)^2\left[G_{\theta\varphi} - G_\theta\left(D+\frac{\rho_\varphi}{\rho}\right) + G_\varphi\,\frac{\rho_\theta}{\rho}\right]$$

$$- (2F)^2G_\varphi(CG_\theta + B^2DG_\varphi) + \rho^{\gamma+1}S\left(\gamma\,\frac{\rho_\varphi}{\rho}+\frac{S'}{S}\,G_\varphi\right) \qquad (20)$$

r momentum:

$$(ABG_\varphi)^2F_{\theta\theta}$$

$$= (AB)^2\left[F_\theta G_\theta G_{\varphi\varphi} - (F_\theta G_\varphi + F_\varphi G_\theta)G_{\theta\varphi} + F_\varphi G_\varphi G_{\theta\theta} - G_\theta{}^2F_{\varphi\varphi} + 2G_\theta G_\varphi F_{\theta\varphi}\right]$$

$$- 2F(A^2G_\theta{}^2+B^2G_\varphi{}^2) - (F_\varphi G_\theta - F_\theta G_\varphi)\left[B^2\left(2A^2C-C+A^2\,\frac{\rho_\theta}{\rho}\right)G_\varphi\right.$$

$$\left. - A^2\left(2B^2D-D+B^2\,\frac{\rho_\varphi}{\rho}\right)G_\theta\right] \qquad (21)$$

It has been stipulated that F is to vanish on the surface of the body. It would appear, then (see eqs. (17)), that the velocities v and w must also be zero there. This is not generally the case, so the derivatives G_φ and G_θ must become infinite on the body. The singular nature of the derivatives of G at the body is evidence of the previously mentioned singular behavior of the entropy near the body, since S and G are functionally related (see eq. (16)).

THE INITIAL CONDITIONS

The shock wave is taken to be an elliptic cone of the family described by the second of equations (4). The value of θ at the shock cone is designated θ_o. The equation of this conical surface is

$$\Gamma(x,y,z) = x^2 - \frac{y^2}{b_1^2} - \frac{z^2}{a_1^2} = 0 \tag{22}$$

The component of the free-stream Mach number normal to the shock wave is

$$M_N = \frac{M_x\left(\frac{\partial\Gamma}{\partial x}\right) + M_y\left(\frac{\partial\Gamma}{\partial y}\right) + M_z\left(\frac{\partial\Gamma}{\partial z}\right)}{\sqrt{\left(\frac{\partial\Gamma}{\partial x}\right)^2 + \left(\frac{\partial\Gamma}{\partial y}\right)^2 + \left(\frac{\partial\Gamma}{\partial z}\right)^2}} \tag{23}$$

where M_x, M_y, M_z are the x, y, and z components of the free-stream Mach number. When rewritten in terms of the sphero-conal coordinates, equation (23) becomes

$$\frac{M_N}{M_\infty} = \sin\theta_o\cos\alpha\cos\beta\sqrt{\frac{(1-k^2\cos^2\theta_o)(1-k'^2\cos^2\varphi)}{k^2\sin^2\theta_o + k'^2\sin^2\varphi}}$$

$$- \sin\theta_o\sin\varphi\cos\alpha\sin\beta\sqrt{\frac{1-k^2\cos^2\theta_o}{k^2\sin^2\theta_o + k'^2\sin^2\varphi}}$$

$$- \cos\varphi\sin\alpha\frac{k^2\sin\theta_o\cos\theta_o}{\sqrt{k^2\sin^2\theta_o + k'^2\sin^2\varphi}} \tag{24}$$

The angles of attack and yaw, α and β, and the x, y, and z components of Mach number are shown in figure 3. Note that the axes are fixed in the shock wave and that their origin is at the cone vertex.

Expressions are required for evaluating velocity components, density, pressure, and the stream functions just behind the shock wave. The oblique shock relations (see, e.g., ref. 18) along with equation (24) and equations (17) are utilized in the writing of these expressions. In the following paragraphs the equations that apply only at the shock will be clearly indicated so as to distinguish them from such general relations as may appear in the analysis.

The velocity components u and w lie in a plane tangent to the shock, just ahead of the shock. They therefore undergo no change through the shock, so that at $\theta = \theta_o$

A 3 8 5

$$u = \cos\theta_o \cos\alpha \cos\beta \sqrt{1-k'^2\cos^2\varphi} + \sin\theta_o \sin\varphi \cos\alpha \sin\beta + \cos\varphi \sin\alpha \sqrt{1-k^2\cos^2\theta_o} \qquad (25)$$

$$w = \cos\theta_o \cos\alpha \cos\beta \frac{k'^2 \sin\varphi \cos\varphi}{\sqrt{k^2\sin^2\theta_o + k'^2\sin^2\varphi}} - \sin\theta_o \sin\varphi \cos\alpha \sin\beta \sqrt{\frac{1-k'^2\cos^2\varphi}{k^2\sin^2\theta_o + k'^2\sin^2\varphi}} - \sin\varphi \sin\alpha \sqrt{\frac{(1-k^2\cos^2\theta_o)(1-k'^2\cos^2\varphi)}{k^2\sin^2\theta_o + k'^2\sin^2\varphi}} \qquad (26)$$

The velocity v and the density and pressure are found from the shock relations to be

$$v = -\frac{(\gamma-1)M_N^2 + 2}{(\gamma+1)M_N M_\infty} \qquad (27)$$

$$\rho = \frac{(\gamma+1)M_N^2}{(\gamma-1)M_N^2 + 2} \qquad (28)$$

$$p = \frac{2\gamma M_N^2 - (\gamma-1)}{\gamma(\gamma+1)M_\infty^2} \tag{29}$$

where M_N is represented by equation (24).

If equations (27), (28), and the first of equations (17) are combined, the result is

$$\rho v = -\frac{M_N}{M_\infty} = -2BFG_\varphi \tag{30}$$

If the second equality is taken in equation (30), and if equation (24) is inserted for M_N/M_∞ an expression is obtained which can be solved for G_φ, valid, of course, only at $\theta = \theta_o$; that is,

$$G_\varphi = \frac{1}{2F}\left(\cos\theta_o\cos\alpha\cos\beta\sqrt{1-k^2\cos^2\theta_o}\right.$$
$$- \cos\theta_o\sin\varphi\cos\alpha\sin\beta\sqrt{\frac{1-k^2\cos^2\theta_o}{1-k'^2\cos^2\varphi}}$$
$$\left. - \cos\varphi\sin\alpha\frac{k^2\sin\theta_o\cos\theta_o}{\sqrt{1-k'^2\cos^2\varphi}}\right) \tag{31}$$

at $\theta = \theta_o$. The form of the functions F and G at the shock is still, to some extent, arbitrary. If it is asked that G be equal to φ on the shock, then this can be accomplished by setting

$$F = \frac{1}{2}\left(\sin\theta_o\cos\alpha\cos\beta\sqrt{1-k^2\cos^2\theta_o}\right.$$
$$- \cos\theta_o\sin\varphi\cos\alpha\sin\beta\sqrt{\frac{1-k^2\cos^2\theta_o}{1-k'^2\cos^2\varphi}}$$
$$\left. - \cos\varphi\sin\alpha\frac{k^2\sin\theta_o\cos\theta_o}{\sqrt{1-k'^2\cos^2\varphi}}\right) \tag{32}$$

The streamlines, upon which entropy is constant, converge near the body and come together at B. Thus all values of entropy exist at B, a singular point. The point E is also singular by reasons of symmetry. The entropy therefore undergoes rapid change in the vicinity of the body, thus leading to the notion of an entropy layer. The streamline emanating from the shock at C impinges upon the body at A, and follows the body surface around to B. The velocity v is normal to the body at points A and B, and so it is zero there. The body can be completely determined, then, by plotting the points on AC and BD where v vanishes and by noting the points where curves S versus φ (θ = const.) cross the line $S(\theta = \theta_o, \varphi = 0) = \text{const.}$

THE NUMERICAL ANALYSIS

A 3 8 5

The conical shock problem is solved here by two methods, one using the stream-function formulation of the equations of motion and the other using the velocity-component formulation. The two procedures are programmed for electronic computers, and for convenience they are termed the "stream-function program" and the "velocity-entropy program." Descriptions of the computer programs are given in the following sections, along with a brief discussion of their specific application and limitations.

The Stream-Function Program

This program has been set up for an Electro-Data 205 Electronic Data Processing Machine. The program is in most ways identical to the one with which the calculations were performed in reference 14, with the extenstion here to include angles of attack or yaw. Equations (19) to (21), along with equations (25) to (28), (33) to (36), and (38) to (42), define the problem.

For a given case, values are prescribed for

θ_o, b_1/a_1 } shock-wave geometry

M_∞ free-stream Mach number

γ adiabatic exponent

α angle of attack

β angle of yaw

$\Delta\theta$ increment in θ, a positive quantity

n number of points

The increment $\Delta\varphi$ is found from the tabulation below, which is incorporated in the computer program.

α	β	$\Delta\varphi$	Range of φ
0	0	$\pi/2n$	$(\Delta\varphi/2) \leq \varphi \leq (\pi/2) - (\Delta\varphi/2)$
0	$\neq 0$	π/n	$-(\pi/2) + (\Delta\varphi/2) \leq \varphi \leq (\pi/2) - (\Delta\varphi/2)$
$\neq 0$	0	π/n	$(\Delta\varphi/2) \leq \varphi \leq \pi - (\Delta\varphi/2)$

A 3 8 5 In practice 15 or 20 points are used, but as few as 10 and as many as 60 have been used in some cases. The size of $\Delta\theta$ is chosen so that 8 or 10 increments are taken to get to the body. Cases have been run with as few as 2 and up to 50 or 60 steps to the body. No particular difficulty is encountered in using the very small increments. This is in contrast with the calculations of reference 12, where an inherent instability limits the number of steps to the body.

The calculations are arranged according to the outline below.

Step 1a.- Compute initial values of ρ, F, G, F_θ, and G_θ at the shock wave using the input values of θ_o, b_1/a_1, etc.

Step 1.- Compute the derivatives ρ_φ, F_φ, G_φ, $F_{\theta\varphi}$, $G_{\theta\varphi}$, $F_{\varphi\varphi}$, and $G_{\varphi\varphi}$ numerically. Compute S and S'/S. Solve the equations of motion for ρ_θ, $F_{\theta\theta}$, and $G_{\theta\theta}$. Calculate the "externally iterated" value of ρ, designated ρ_{it}, using the formula

$$\rho_{it}^{(n)} = \rho_{it}^{(n-1)} - \frac{\Delta\theta}{2}\left[\rho_\theta^{(n)} + \rho_\theta^{(n-1)}\right] \tag{43}$$

(At the shock, $\rho_{it} = \rho$.) It is termed "externally iterated" in that is is computed at each point using only the information at hand, and it is not used in the subsequent extrapolations. The pressure p is computed with the relation $p = \rho_{it}^{\gamma} S$. Pressure, density, and other pertinent flow-field data are now read out of the computer.

Step 2.- Extrapolate ρ, F_θ, and G_θ to the coordinate θ_{n+1} using the formulas

$$\left.\begin{aligned} \rho^{(n+1)} &= \rho^{(n)} - \Delta\theta\rho_\theta^{(n)} \\ F_\theta^{(n+1)} &= F_\theta^{(n)} - \Delta\theta F_{\theta\theta}^{(n)} \\ G_\theta^{(n+1)} &= G_\theta^{(n)} - \Delta\theta G_{\theta\theta}^{(n)} \end{aligned}\right\} \tag{44}$$

Take these values of $F_\theta^{(n+1)}$ and $G_\theta^{(n+1)}$ along with the previously calculated results $F^{(n)}$ and $G^{(n)}$ and extrapolate F and G with the equations

$$\left.\begin{aligned} F^{(n+1)} &= F^{(n)} - \frac{\Delta\theta}{2}\left[F_\theta^{(n)} + F_\theta^{(n+1)}\right] \\ G^{(n+1)} &= G^{(n)} - \frac{\Delta\theta}{2}\left[G_\theta^{(n)} + G_\theta^{(n+1)}\right] \end{aligned}\right\} \tag{45}$$

A 3 8 5

Step 3.- If any values of the stream function F have become negative at $\theta = \theta_{n+1}$ go to step 4. Otherwise repeat steps 1, 2, and 3.

Step 4.- Some values of F are negative at $\theta = \theta_{n+1}$. Recall the flow data for $\theta = \theta_n$ and extrapolate to the body with the following equations. The subscript b indicates results on the body.

$$\left.\begin{aligned} \Delta\theta_b &= \frac{F^{(n)}}{F_\theta^{(n)}} \\ \theta_b &= \theta_n - \Delta\theta_b \end{aligned}\right\} \tag{46}$$

$$\left.\begin{aligned} y_b &= \frac{\sin\varphi \sin\theta_b}{\cos\theta_b\sqrt{1 - k'^2\cos^2\theta}} \\ z_b &= \frac{\cos\varphi}{\cos\theta_b}\sqrt{\frac{1 - k^2\cos^2\theta_b}{1 - k'^2\cos^2\varphi}} \end{aligned}\right\} \tag{47}$$

$$\left.\begin{aligned} p_b &= p^{(n)} - \Delta\theta_b p_\theta^{(n)} \\ p_\theta^{(n)} &= p^{(n)}\left[\gamma \frac{\rho_\theta^{(n)}}{\rho^{(n)}} + \left(\frac{S'}{S}\right)^{(n)} G_\theta^{(n)}\right] \end{aligned}\right\} \qquad (48)$$

Note that y_b and z_b are actually ratios $(y/x)b$ and $(z/x)b$, and are, as such, projections of the body coordinates r, θ_b, and φ onto a plane $x = 1$. These coordinates, along with p_b, are now read out of the computer and the case is finished.

The order of procedure discussed in the foregoing paragraphs can be seen graphically in figure 5, which is a simplified flow chart of the computing program.

Note in step 3 of the foregoing outline that the integration is stopped as soon as the stream function F changes sign anywhere on the coordinate ellipse θ_{n+1}. The body is then located by linear extrapolation of the data at θ_n to the place where F vanishes. In cases where the ellipse θ_n is markedly different in shape from the body, the extrapolated distance, $\Delta\theta_b$, may be excessively large, resulting in an inaccurate representation of the body. This situation occurs for very large values of α or β, or for small values of b_1/a_1, or for small Mach numbers. The computer program was not readily amenable to modification to overcome this difficulty, which in general prevented close analysis of the entropy layer on the body. A number of cases were calculated using this program, and limits on parameter values were generally established from comparison of results with calculations using the velocity-entropy program. The latter program has been set up so as to overcome the difficulty discussed above, and it is described in the following section.

The Velocity-Entropy Program

This program was set up for an IBM 704 electronic computer for the purposes of studying the entropy layer on conical bodies, and as an independent check on the stream-function program. The velocity formulation of the equations of motion, equations (7), is used here. This formulation is numerically less involved than the stream-function formulation. Only first derivatives must be taken numerically in the velocity formulation, for example, whereas second derivatives are required in the other. The velocity-entropy program is the more versatile of the two in that the range of φ is arbitrary and need not be precisely $\pi/2$ or π radians. It is the more difficult of the two to use, however, in that the body is found by an analysis of the entropy, which cannot easily be programmed for the computer. It is not intended as a production program and only a few cases have been analyzed in detail with its use.

The initial shock-wave data are found from equations (25) to (29) with prescribed values of θ_o, b_1/a_1, M_∞, γ, α, β, $\Delta\theta$, and n. The number of points n may be in the range $7 \leq n \leq 50$. (The lower limit 7 is dictated by the numerical differentiation scheme that is employed here.) The range of φ is also specified along with θ_o, b_1/a_1, etc., by prescribing values of L_1 and L_2. These two quantities are angles and are put into the relation $\Delta\varphi = (L_2 - L_1)/n$. The values of φ are then taken at intervals $\Delta\varphi$ in the range $(L_1 + \Delta\varphi/2) \leq \varphi \leq (L_2 - \Delta\varphi/2)$. For $\alpha = \beta = 0$ it is usual to take $L_1 = 0$ and $L_2 = 90^o$, but different values may be used if desired. An outline of the computing procedure is presented next.

Step 1a.- Compute initial values of u, v, w, p, and ρ at the shock wave using the given values of θ_o, b_1/a_1, etc. Compute $S = p/\rho^\gamma$.

Step 1.- Calculate numerically the derivatives u_φ, v_φ, w_φ, ρ_φ, S_φ. Calculate u_θ, v_θ, w_θ, ρ_θ, and S_θ from the equations of motion. Compute ρ_{it} using equation (43). Compute pressure p using the formula $p = \rho_{it}{}^\gamma S$. Read current values, at $\theta = \theta_n$, of u, v, w, p, ρ, and S out of the computer.

Step 2.- Extrapolate velocities, ρ, and S to the next θ coordinate using the formulas

$$\left.\begin{aligned} u^{(n+1)} &= u^{(n)} - \Delta\theta u_\theta^{(n)} \\ v^{(n+1)} &= v^{(n)} - \Delta\theta v_\theta^{(n)} \\ w^{(n+1)} &= w^{(n)} - \Delta\theta w_\theta^{(n)} \\ \rho^{(n+1)} &= \rho^{(n)} - \Delta\theta \rho_\theta^{(n)} \\ S^{(n+1)} &= S^{(n)} - \Delta\theta S_\theta^{(n)} \end{aligned}\right\} \qquad (49)$$

Step 3.- If any values of the velocity v have become positive at $\theta = \theta_{n+1}$ go to step 4. Otherwise repeat steps 1, 2, and 3.

Step 4.- Some values of $v^{(n+1)}$ have become positive. Recall the flow-field results for the station $\theta = \theta_n$ and continue the integration using one of the two options A and B. The option choice is specified along with the initial data θ_o, b_1/a_1, etc.

Option A.- Calculate a new value for $\Delta\theta$. The new $\Delta\theta$ is some fraction, say 1/5, of the original value. The integration is continued now (steps 1 and 2), and instead of using all n data points at once, several smaller segments are used. The segments may overlap, and the integration proceeds on each segment until all values of S are greater than the value calculated to exist on the body, or until a pre-set number of steps have been taken, or until the calculation breaks down as evidenced by negative S or ρ values. The size of the small segments, the number of points between the first points of succeeding segments, and the size of the new $\Delta\theta$ are all specified with the initial parameters.

Option B.- This process starts at $\theta = \theta_n$ in the flow field and uses a reduced value of $\Delta\theta$, as in option A. It depends on the entropy variations being of the form shown in figure 6, a situation that prevails for elliptic cone shocks at $\alpha = \beta = 0$ in the region $0 \leq \varphi \leq 90^\circ$, or circular cone shocks at finite angles β in the range $-90^\circ \leq \varphi \leq 90^\circ$. Observe in figure 6 that the derivative S_φ is negative over most of the flow field, but that zero values begin to appear as the integration proceeds. The points of zero slope are labeled S_1 and S_2. If the data to the right of point S_2 on the θ_{n+2} curve are used in extrapolating to the coordinate θ_{n+3}, numerical difficulties arise due to extreme values of S_φ in this region, and due also to the fact that the velocity v passes through zero near S = 0. Divisions by very small values of v can introduce large errors in the subsequent calculation of S, ρ, etc., from the equations of motion. These same difficulties appear in data to the left of points S_1. The technique in option B is to continue the integration from θ_n, but to retain, at the extrapolation step, only the data lying in the region between points S_1 and S_2 on the entropy curve. The integration is continued in this manner until erroneous negative values of ρ or S occur within the range $\varphi(S_1)$ to $\varphi(S_2)$, or until all values of S are greater than the body value.

The body is found with either option by converting the $\varphi - \theta$ coordinates of places where the entropy curves cross the line of constant entropy that represents the body entropy to y_b and z_b, using equations (47).

No flow chart is presented for the velocity-entropy program. It is identical in concept to the one shown in figure 4 for the stream-function program.

As has been indicated, the numerical data near the body are subject to the ravages of division by zero and abrupt changes in slope of quantities whose derivatives must be obtained numerically. These problems occur to the largest extent in the region nearest the entropy singularity, and have a physical basis in the fact that the entropy does indeed change very

rapidly in a thin region near the body, and most rapidly near and at the singular point. There does not seem to be any general numerical procedure suitable for machine programming by which the calculations can be performed with assurance in this region. Results can usually be obtained over the first portion of a body, but only with difficulty over the region ending at the singularity, even with the devices of options A and B. In a given case it is usually necessary to recompute several times, using both options A and B, and with various lengths of segment size in option A in order to get a reasonably complete picture of the entropy variation in the region near the entropy singularity.

PRESENTATION OF RESULTS

Preliminary Calculations and Comparisons

Preliminary calculations for elliptic conical shock waves at zero angles of incidence are given in reference 14. The main purpose of these calculations was to study the stability and convergence of the numerical process, and the effect on the results of variations of γ and M_∞. It was found that the calculations are stable and convergent for small increments $\Delta\theta$. The bodies that support elliptic conical shocks are themselves somewhat flatter than elliptic cones. The change in body shape and surface pressure with changing Mach number is as might have been anticipated. The limiting case of $\gamma = 1$, $M_\infty \to \infty$ corresponds to the so-called Newtonian plus centrifugal theory. A machine result calculated with $\gamma = 1.001$ and $M_\infty = 10{,}000$ is compared with the simple Newtonian theory, which states that the surface pressure is proportional to the square of the sine of the local body angle. Laval, reference 19, has calculated pressures on conical bodies in the limit $\gamma = 1$, $M_\infty = \infty$. He presents a result for the case of $\theta_o = 30^o$, $b_1/a_1 = 0.6$, and $\alpha = \beta = 0$, the same case used for the comparison in reference 14. These results are brought together in figure 7.

Initial comparisons of calculations using the two computer programs described in the present report were made with the case of $\theta_o = 30^o$, $b_1/a_1 = 0.6$, $M_\infty = 6$, $\gamma = 1.4$, and $\alpha = \beta = 0$. The computed body shape and surface pressure are shown in figure 8. Observe that the results of the two computer programs differ by a small amount. Another comparison of the two computer methods is shown in figure 9 for the case of a circular shock wave, $\theta_o = 30^o$, at an angle of yaw of 20^o, and with $\gamma = 1.4$ and $M_\infty = 10$. This is the case reported in reference 13. Again, there is a slight discrepancy between the results of the two machine procedures. The velocity-entropy calculation agrees closely with the result of reference 13, except on the leeward side, which is remarkable when it is realized that Radhakrishnan's work was carried out on a desk computer. The differences in the machine calculated results can probably be ascribed in part to differences in programming procedures, and to the numerical difficulty associated with the body extrapolation process of the stream-function program. The differences are not great, however, but the velocity-entropy program is presumed to give the more precise results.

The variations of entropy and velocity components with the coordinate φ for the case shown in figure 8 are presented in figures 10 to 13. The streamline pattern in the crossflow is shown in figure 14.

Stocker has calculated conical bodies by a two-stream-function technique wherein the stream functions are independent rather than dependent variables. No report has been published by Stocker, as yet, but the results of one of his calculations, as given in reference 20, are shown for comparison in figure 8. His results agree well with calculations using the velocity-entropy program.

Mauger, reference 21, has applied complex variable theory and the method of Garabedian (ref. 22) to compute bodies that support conical shock waves. He presents a calculation for an elliptic conical shock wave, and the results of the same case as computed by the method of Stocker. These are shown in figure 15, along with a calculation by the velocity-entropy program. The agreement is very good. Note that pressure has been plotted against the angle ψ where $\psi = \text{arc tan}(y_b/z_b)$.

An interesting facet of the present work is the inclusion of calculation of a so-called "externally iterated" density. (See eq. (43) and also ref. 12.) Pressures were computed at the place $\varphi = 0$ on the body for the case shown in figure 8 using both iterated and uniterated densities. The results differed by about 1.5 percent at that point.

Comparisons With Experimental Data

Various wind-tunnel experiments have been performed on elliptic conical bodies (see, e.g., refs. 23 and 24). The shock supported by an elliptic conical body is not an elliptic cone, and conversely an elliptic conical shock wave will be supported by a body that is not elliptic in cross section. Thus no precise comparison can be made between results of tests on elliptic cones and the calculations that assume an elliptic conical shock wave. Some calculations were performed, however, assuming that the shock waves of references 23 and 24 are elliptic cones. The resulting bodies and pressures are shown with the experimental data in figures 16 and 17. Note that pressures are plotted against the angle ψ where $\psi = \text{arc tan}(y_b/z_b)$. Two attempts were made in calculating the conical body to compare with the actual cone tested in the $M_\infty = 6$ experiments of reference 24, and both results are shown in figure 17.

Comparison With an Approximate Theory

A case was calculated for a circular conical shock wave with $\theta_o = 30^\circ$, $M_\infty = 10$, $\gamma = 1.4$, $\alpha = 0$, and $\beta = 10^\circ$, using the stream-function program. The resulting body was almost circular in cross section, and it

was used as the basis of a computation using the first-order yawed-cone theory given in reference 6. Relevant parameters are, in the notation of reference 6, $M_\infty = 10$, $\theta_s = 26.5^\circ$, $\epsilon = 0.1575$, and $\delta = \beta = 0.1745$. The surface pressure, calculated with respect to body axes, is

$$p_b = 0.217[1 + 0.584 \cos(\bar{\varphi} + 90^\circ)] \tag{50}$$

This expression is converted to shock-fixed axes by use of the relation

$$\tan(\bar{\varphi} + 90^\circ) = \frac{\bar{x} + (\delta - \epsilon)}{\bar{x}} \tan(\varphi + 90^\circ) \tag{51}$$

where

$$\bar{x} = \tan^{-1}\theta_s \cos(\bar{\varphi} + 90^\circ) \tag{52}$$

The machine-computed surface pressure and the approximate result are shown in figure 18. These calculations are slightly inconsistent in that the machine computation was carried out using $\gamma = 1.4$, whereas the tables, reference 6, use the value $\gamma = 1.405$.

Systematic Variation of Parameters

A number of cases have been calculated with the stream-function program, wherein one of the initial parameters was systematically varied while the others were held fixed. The accuracy of these calculations was then checked by comparing a few cases with computations performed using the velocity-entropy program. Each of the two programs has presented difficulties which limit the quantity and quality of obtainable results. The stream-function program produces accurate results only where the increment $\Delta\theta_b$ is small over the whole extrapolation region. This, for practical reasons, places lower bounds on M_∞ and b_1/a_1 and upper bounds on the angles α and β. This problem has been avoided in the velocity-entropy program, but the analysis of the entropy data is very time-consuming, and so the number of cases that can reasonably be considered is small. The results presented here agree closely by the two computer programs.

There are many ways in which the initial parameters can be systematically varied. No attempt is made here to do more than sample a few combinations, however. The cases presented are intended mainly to illustrate numerical techniques. The parameter combinations that have been chosen are summarized in tables I to IV, along with the numbers of the figures where the results are plotted.

CONCLUDING REMARKS

The inverse method has been applied to the problem of calculating bodies that support elliptic conical shock waves at finite angles of incidence. The entropy layer at the surface of such bodies has been investigated numerically, also. Two machine computing procedures were employed, and it is presumed that discrepancies of results are due primarily to differences involved in the programming of the two procedures.

The application of two stream functions, one of which vanishes on the body, is a powerful technique in the solution of the three-dimensional conical flow problem. Future attacks on the problems of more complicated three-dimensional flows may employ two stream functions with advantage.

A
3
8
5

The requirement that the shock wave be an elliptic cone makes it difficult to compare calculations with results of actual tests on conical bodies. A logical extension of the present work would be to develop techniques whereby the present assumed shock shapes could be perturbed so that a body of prescribed shape could be found in a few tries.

The major difficulties that have been encountered in the machine computations could be overcome to a large extent if the segmenting processes of the velocity-entropy program and the two-stream-function formulation of the problem were incorporated into a single computing program. Thus good accuracy would be assured, even for very thin conical bodies, and the plotting of final results could be accomplished in a reasonably short time.

Ames Research Center
National Aeronautics and Space Administration
Moffett Field, Calif., July 26, 1960

REFERENCES

1. Busemann, A.: Drucke Auf Kegelförmige Spitzen bei Bewegung mit Uberschallgeschwindigkeit. ZAMM, vol. 9, 1929, p. 496.

2. Taylor, G. I., and Maccoll, J. W.: The Air Pressure on a Cone Moving at High Speeds. - I. Proc. Roy. Soc., series A, vol. 139, Feb. 1933, pp. 278-311.

3. Busemann, A.: Conical Supersonic Flow With Axial Symmetry. Luftfahrtforschung, vol. 19, no. 4, June 1942, pp. 137-144. (Ministry of Aircraft Production R.T.P. Tr. 1958).

4. Staff of the Computing Section (under the direction of Zdenek Kopal): Tables of Supersonic Flow Around Cones. Tech. Rep. 1, Center of Analysis, M. I. T., Cambridge, 1947.

5. Stone, A. H.: On Supersonic Flow Past a Slightly Yawing Cone. Jour. Math. and Phys., vol. 27, no. 1, Apr. 1948, pp. 67-81.

6. Staff of the Computing Section (under the direction of Zdenek Kopal): Tables of Supersonic Flow Around Yawing Cones. Tech. Rep. 3, Center of Analysis, M. I. T., Cambridge, 1947.

7. Staff of the Computing Section (under the direction of Zdenek Kopal): Tables of Supersonic Flow Around Cones at Large Yaw. Tech. Rep. 5, Center of Analysis, M. I. T., Cambridge, 1949.

8. Ferri, Antonio: Supersonic Flow Around Circular Cones at Angles of Attack. NACA Rep. 1045, 1951. (Supersedes NACA TN 2236)

9. Ferri, Antonio: The Linearized Characteristics Method and Its Application to Practical Nonlinear Supersonic Problems. NACA Rep. 1102, 1952. (Supersedes NACA TN 2515)

10. Ferri, Antonio, Ness, Nathan, and Kaplita, Thadeus T.: Supersonic Flow Over Conical Bodies Without Axial Symmetry. Jour. Aero. Sci., vol. 20, no. 8, Aug. 1953, p. 563.

11. Ness, Nathan, and Kaplita, Thaddeus T.: Tabulated Values of Linearized Conical Flow Solutions for Solution of Supersonic Conical Flows Without Axial Symmetry. PIBAL Rep. No. 220, Polytechnic Institute of Brooklyn, Dept. of Aero. Eng. and Appl. Mech., Jan. 1954.

12. Van Dyke, Milton D., and Gordon, Helen D.: Supersonic Flow Past a Family of Blunt Axisymmetric Bodies. NASA Rep. 1, 1959.

13. Radhakrishnan, G.: The Exact Flow Behind a Yawed Conical Shock. Rep. No. 116, The College of Aeronautics, Cranfield, Apr. 1958.

14. Briggs, Benjamin R.: Calculation of Supersonic Flow Past Bodies Supporting Shock Waves Shaped Like Elliptic Cones. NASA TN D-24, 1959.

15. Yih, Chia-Shun: Stream Functions in Three-Dimensional Flows. Reprint No. 158, State Univ. of Iowa, Reprints in Engineering, July-August 1957.

16. Cheng, H. K.: Hypersonic Shock Layer Theory of a Yawed Cone and Other Three-Dimensional Pointed Bodies. WADC TN 59-335, Oct. 1959.

17. Kraus, L.: Diffraction by a Plane Angular Sector. Ph.D. Thesis, New York Univ., May 1955.

A
3
8
5

18. Ames Research Staff: Equations, Tables, and Charts for Compressible Flow. NACA Rep. 1135, 1953.

19. Laval, P.: Ecoulements Newtoniens Sur des Surfaces Coniques en Incidence. La Recherche Aeronautique, no. 73, November- December 1959, pp. 5-16.

20. Van Dyke, Milton D.: Some Numerical Solutions in Hypersonic Flow. Colston Papers, vol XI, Proc. 11th Symposium of the Colston Res. Soc., April 1959.

21. Mauger, F. E.: Steady Supersonic Flow Past Conical Bodies. A.R.D.E. Rep. No. (B)3/60, Fort Halstead, Kent, England, May 1960.

22. Garabedian, P. R.: Numerical Construction of Detached Shock Waves. Jour. Math. and Phys., vol. 36, no. 3, Oct. 1957, pp. 192-205.

23. Chapkis, Robert L.: Hypersonic Flow Over an Elliptic Cone: Theory and Experiment. Hypersonic Research Project Memo. No. 49, Guggenheim Aeronautical Lab., Calif. Inst. of Tech., May 1959.

24. Zakkay, Victor, and Visich, Marian, Jr.: Experimental Pressure Distributions on Conical Elliptic Bodies at $M_\infty = 3.09$ and 6.0. PIBAL Rep. No. 467, Polytechnic Institute of Brooklyn, Dept. of Aero. Eng. and Appl. Mech., March 1959.

TABLE I.- MACH NUMBER VARIATION AT FIXED VALUES OF b_1/a_1 AND WITH $\theta_o = 30^\circ$ AND AT ZERO INCIDENCE

b_1/a_1	Mach no.	Figure
0.6	10, 20, 100	19
.7	5, 10, 20, 100	20
.8	5, 10, 20, 100	21
.9	3, 5, 10, 20, 100	22

TABLE II.- VARIATION OF b_1/a_1 AT FIXED VALUES OF θ_o AND WITH $M_\infty = 10$ AND AT ZERO INCIDENCE

θ_o, deg	b_1/a_1	Figure
10	0.8, 0.9, 1.0	23
15	0.7, 0.8, 0.9, 1.0	24
30	0.6, 0.7, 0.8, 0.9, 1.0	25
40	0.8, 0.9, 1.0	26
50	0.8, 0.9, 1.0	27

TABLE III.- ELLIPTIC CONICAL SHOCK, $\theta_o = 30^\circ$, AND WITH $M_\infty = 10$, AT FINITE INCIDENCE

α, deg	β, deg	Figure
0, 10	0	28
0	0, 5	29

TABLE IV.- CIRCULAR CONICAL SHOCKS WITH $M_\infty = 10$ AND WITH VARIATIONS OF β FOR FIXED VALUES OF θ_o

θ_o, deg	β, deg	Figure
10	0, 2.5	30
15	0, 2.5, 5	31
30	0, 2.5, 5, 10, 20	32
40	0, 5, 10, 20	33
50	0, 5, 10, 20	34

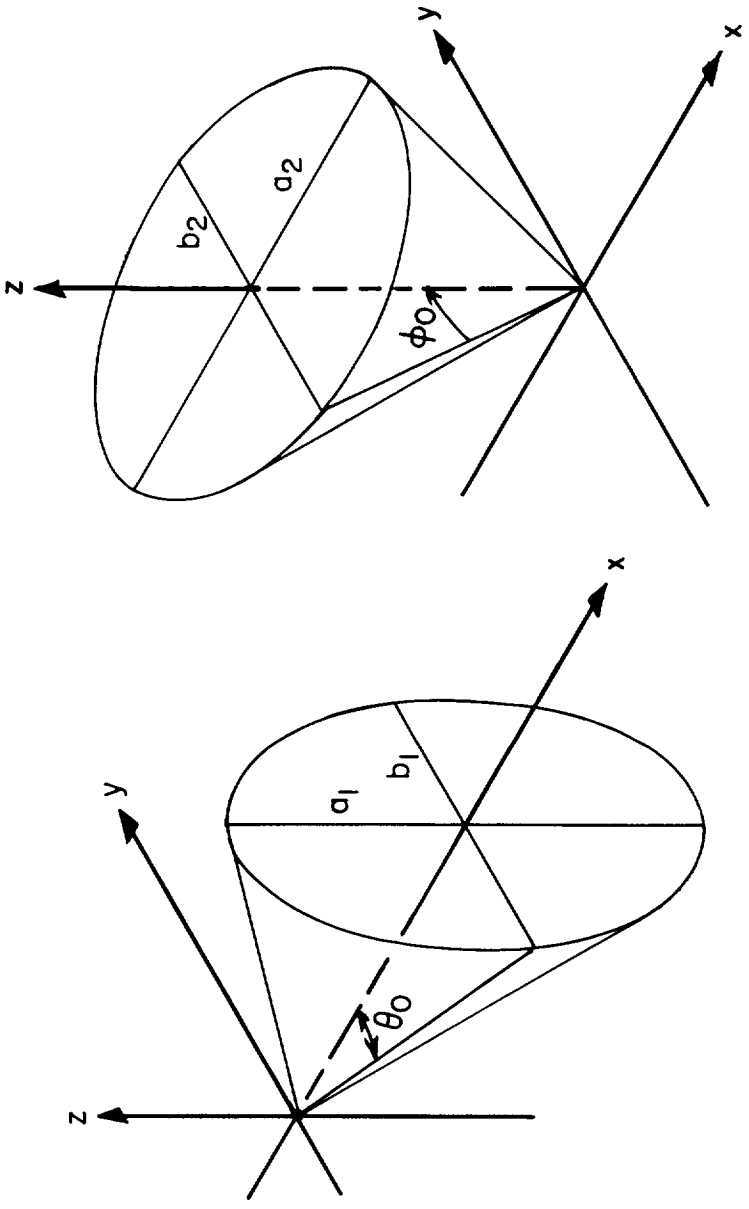

Figure 1.- Surfaces of constant θ and of constant φ.

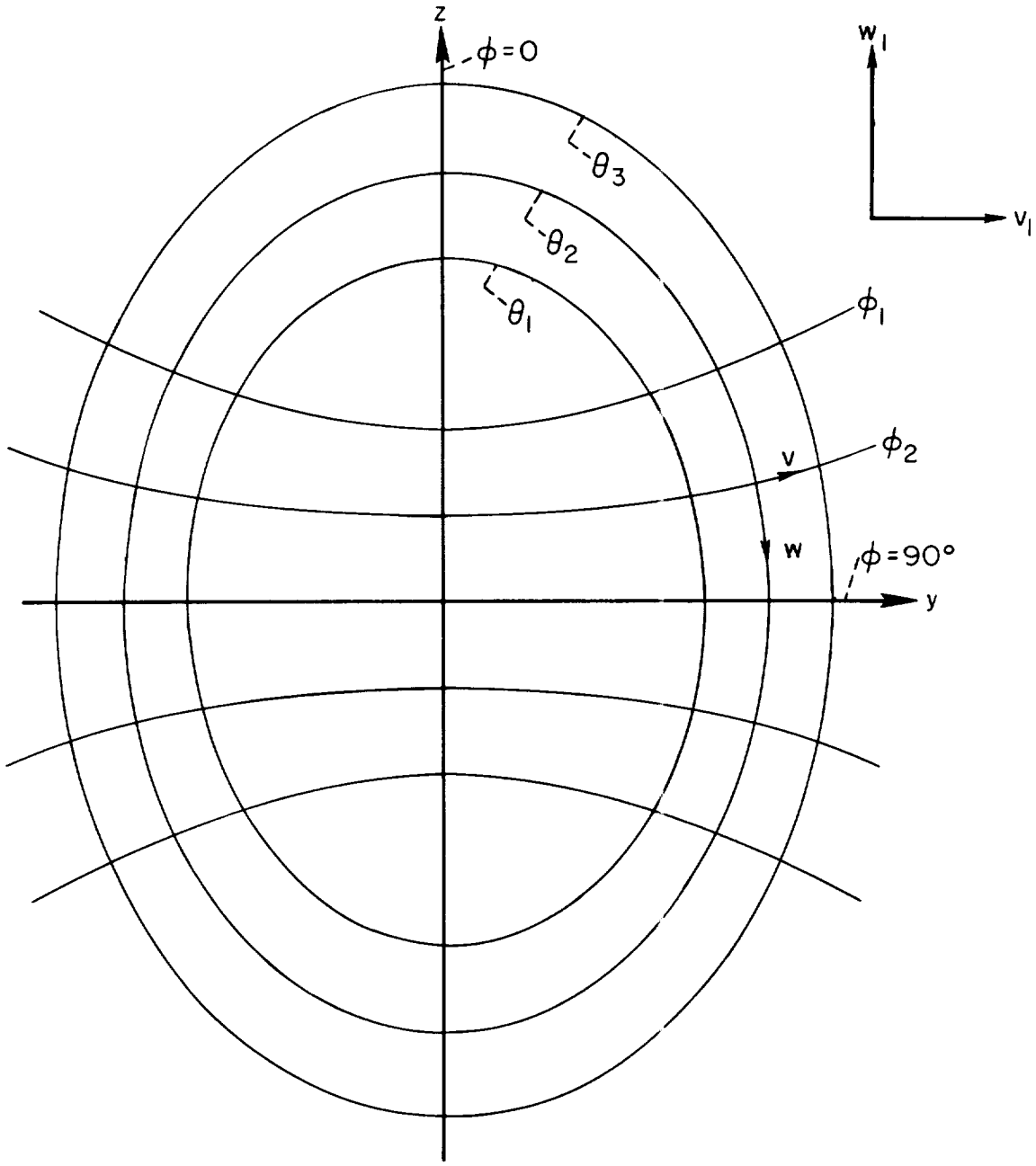

Figure 2.- Velocity components in the sphero-conal and Cartesian coordinate systems.

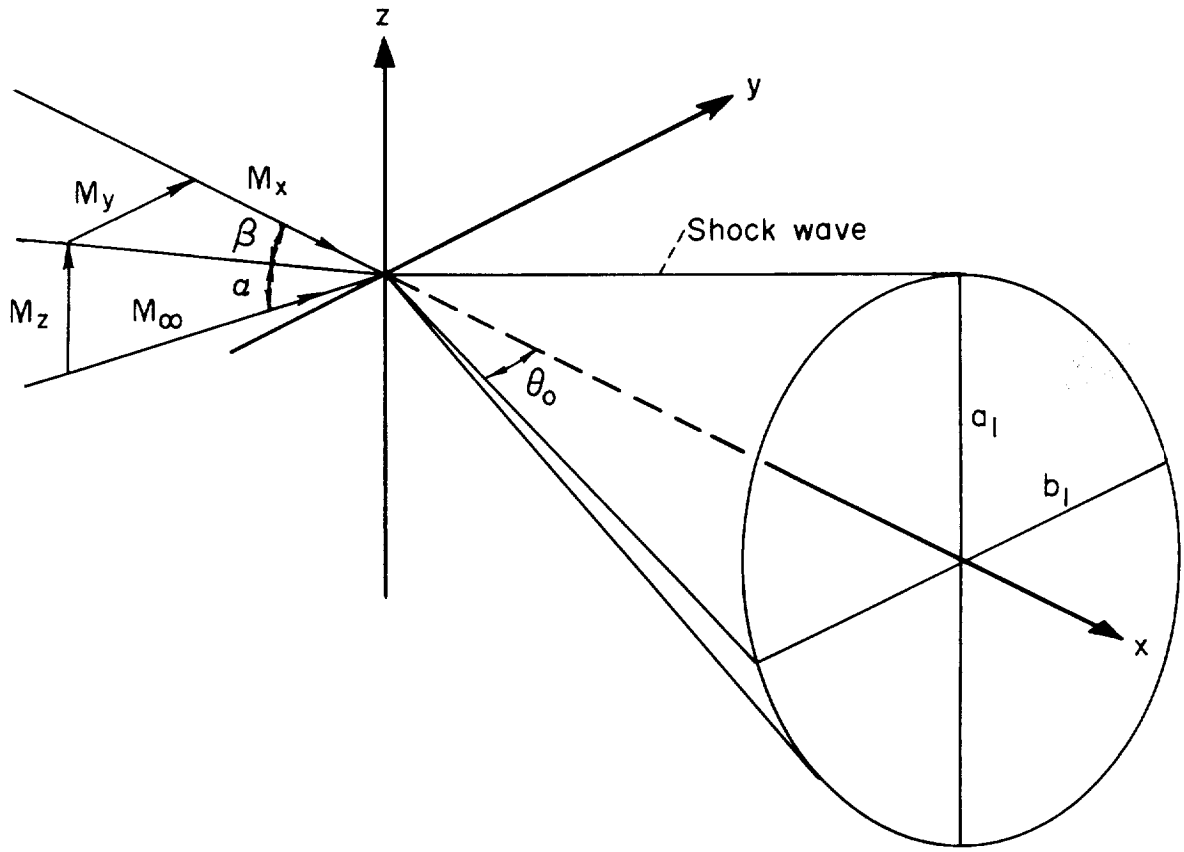

Figure 3.- Cartesian components of the free-stream Mach number.

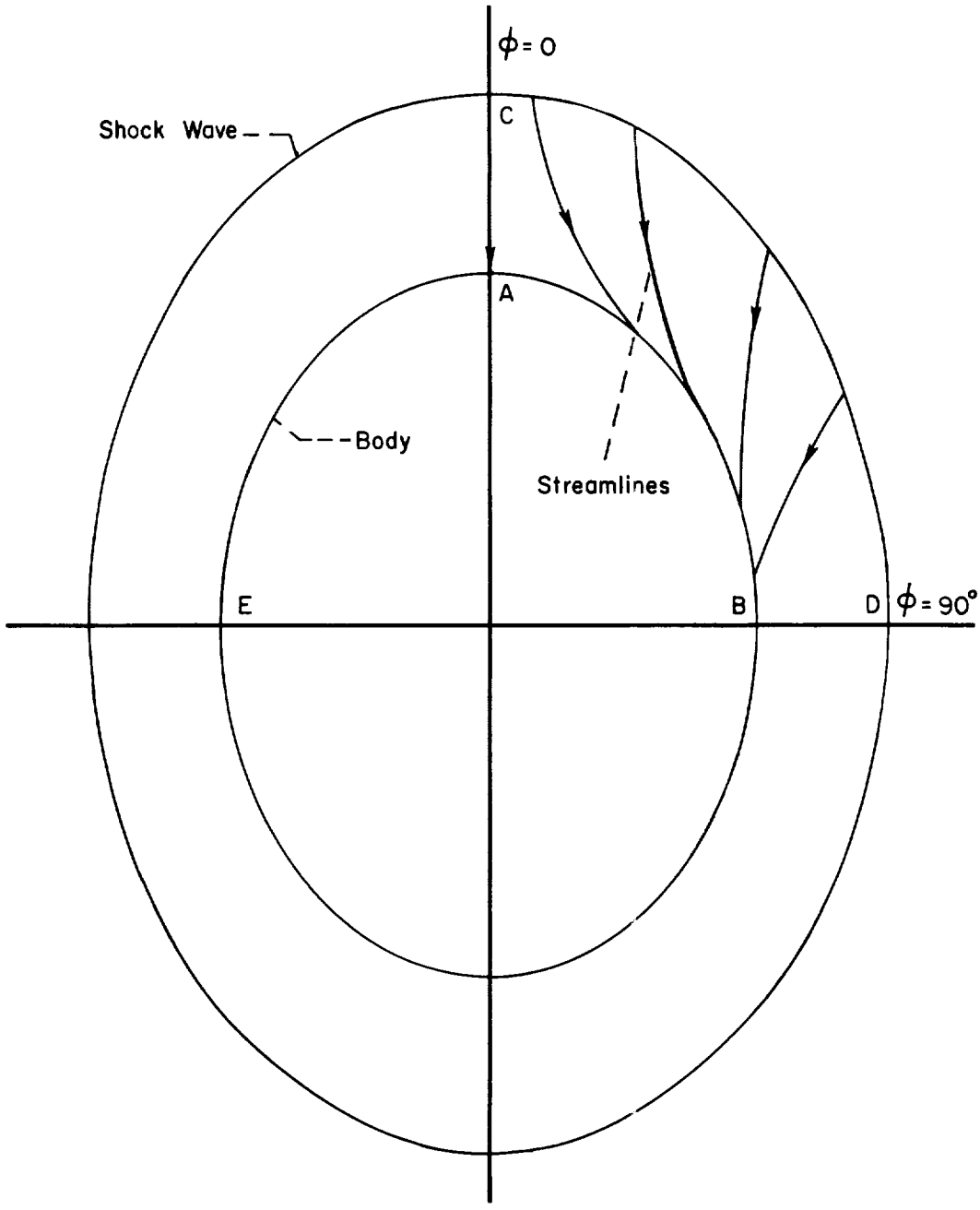

Figure 4.- Streamlines in the conical flow field.

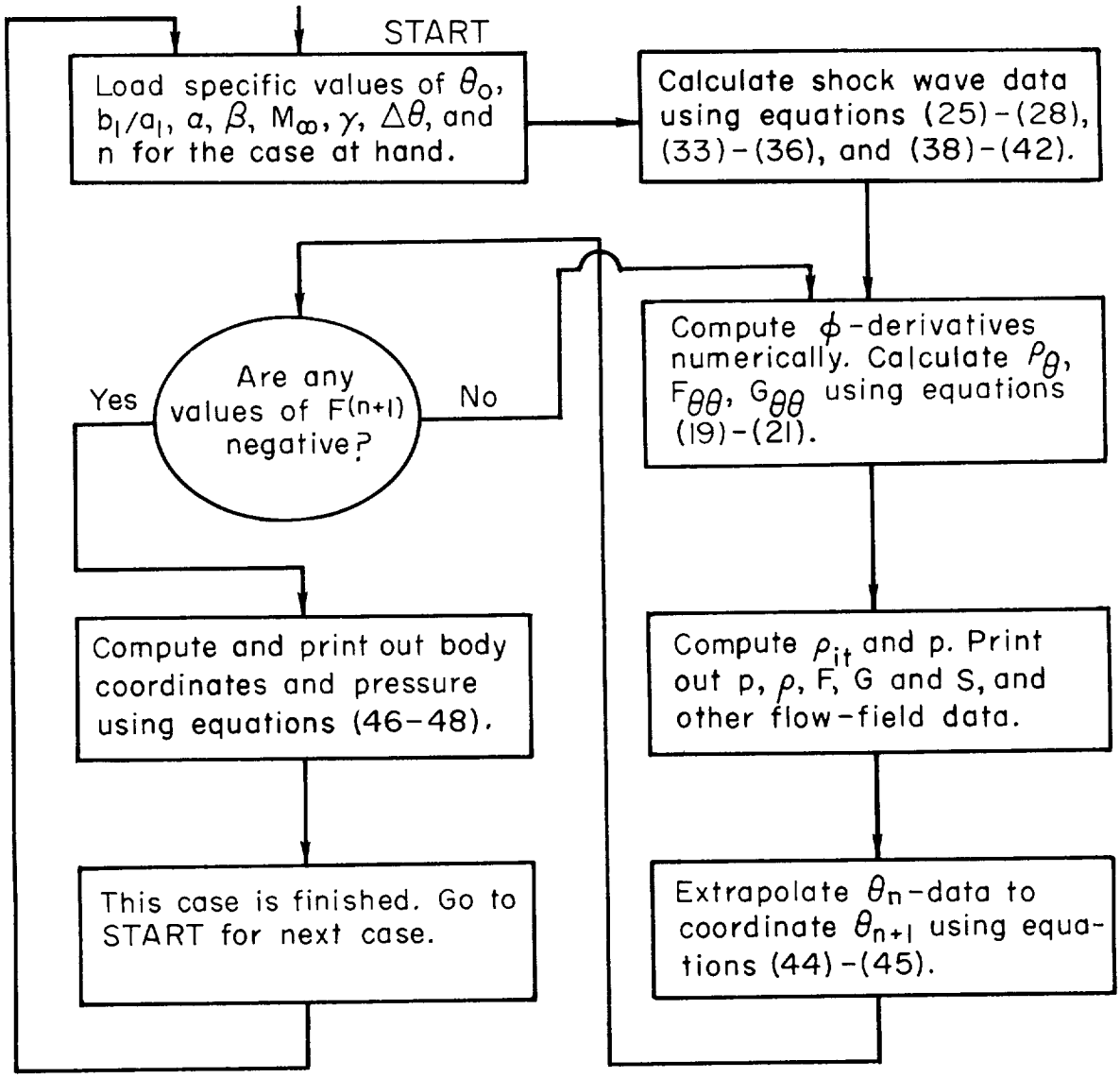

Figure 5.- Flow chart for the stream-function program.

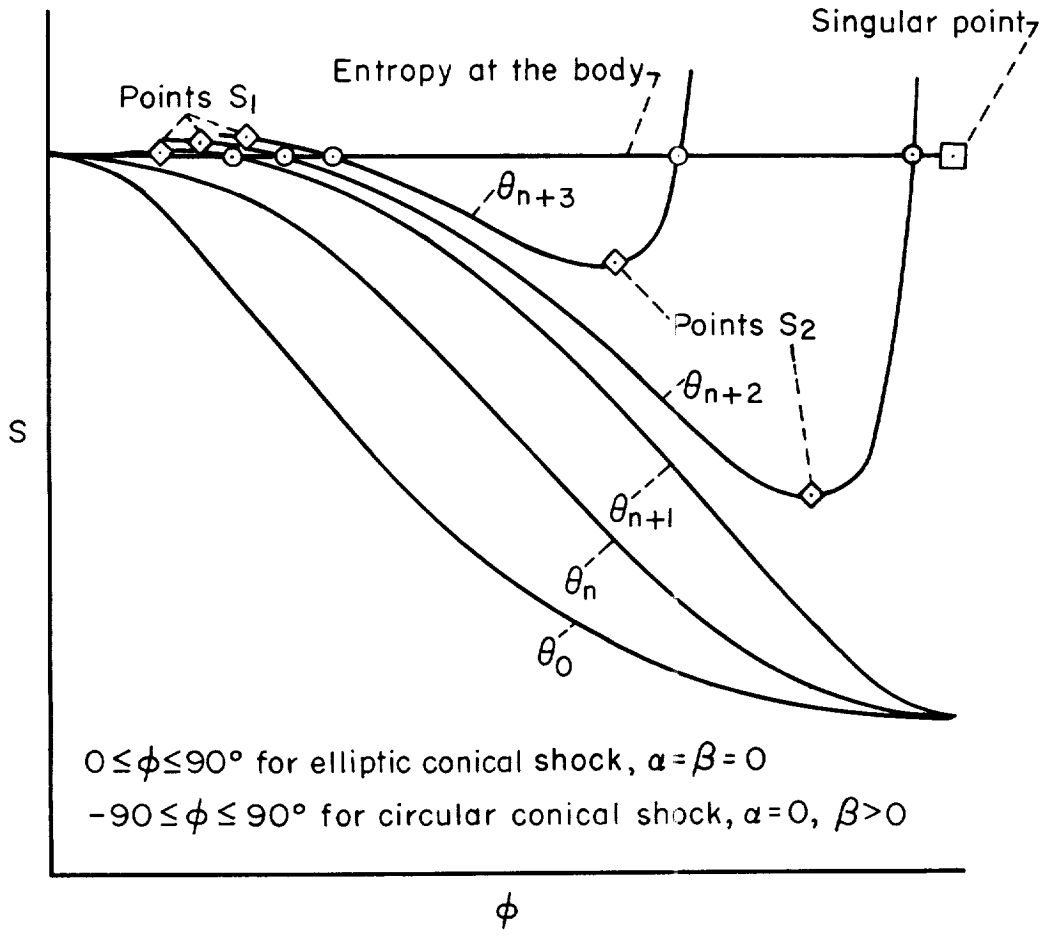

Figure 6.- The variation of entropy with the coordinate φ in the flow field behind elliptic conical shocks at zero incidence, or circular shocks at positive angles β.

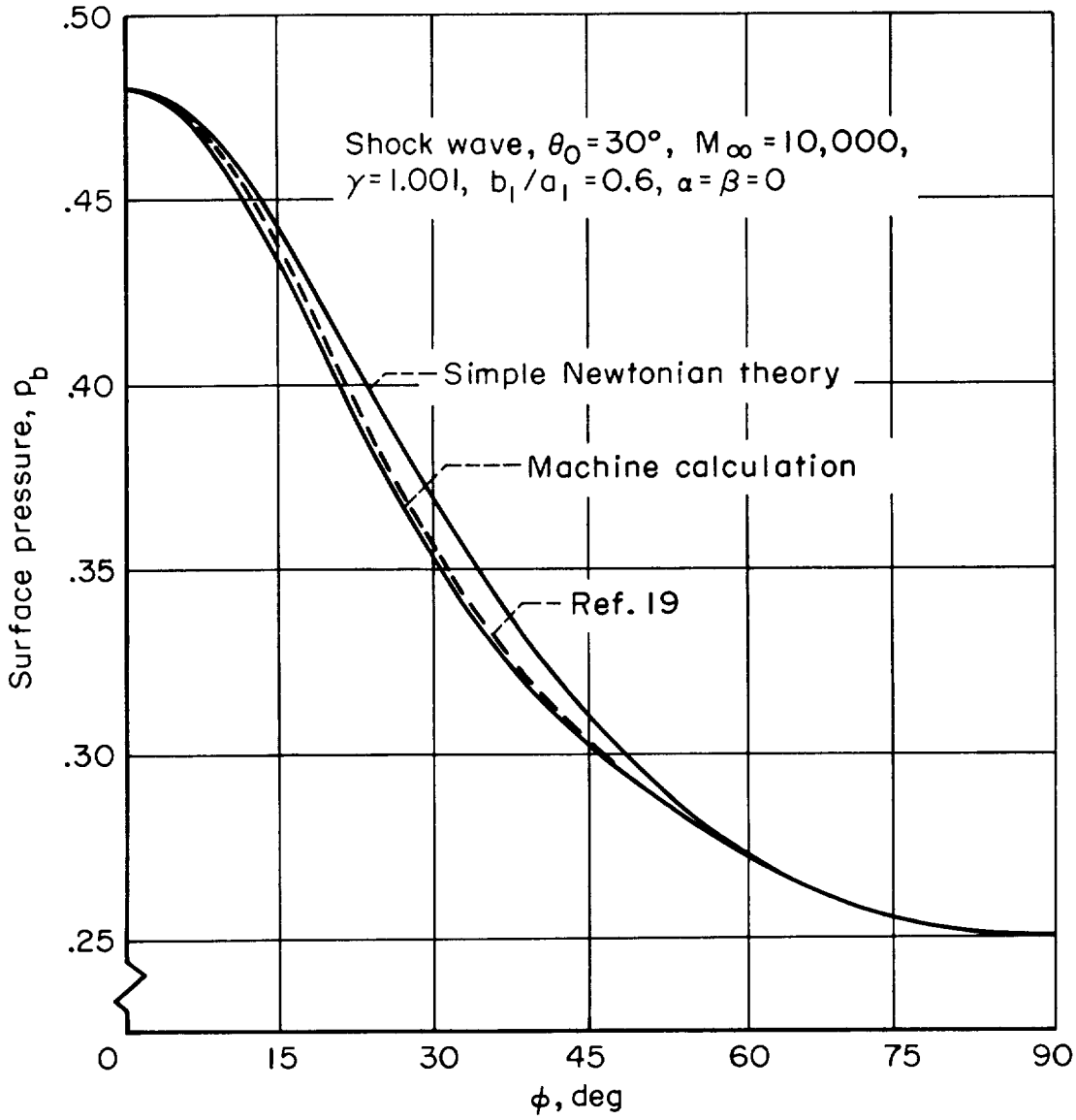

Figure 7.- Comparison of surface pressure in the limiting case of $M_\infty \to \infty$ and $\gamma \to 1$ with simple Newtonian theory and the theory of reference 19.

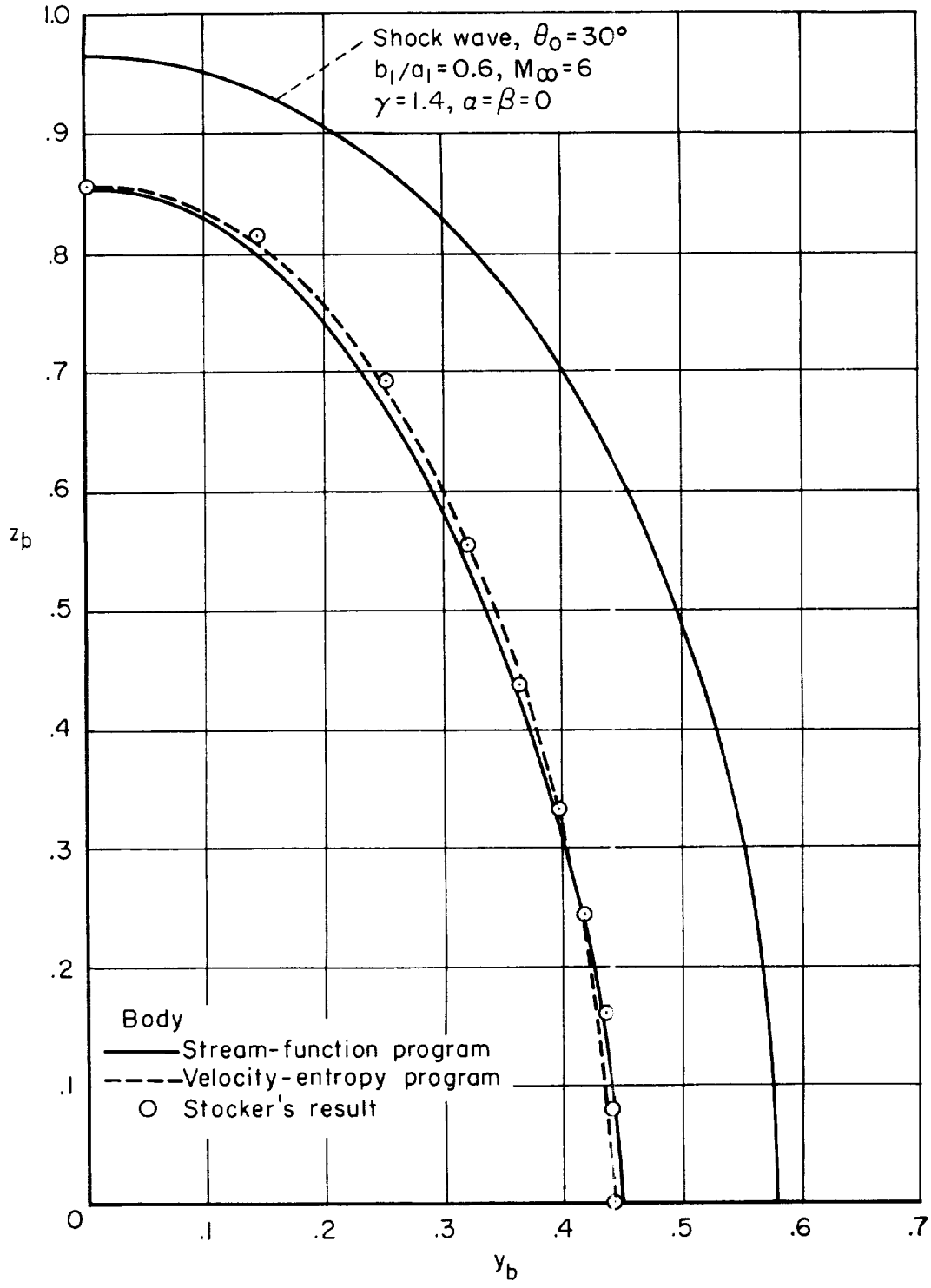

Figure 8.- Comparison of body shapes for an elliptic conical shock wave as calculated by the two computer programs and the method of Stocker.

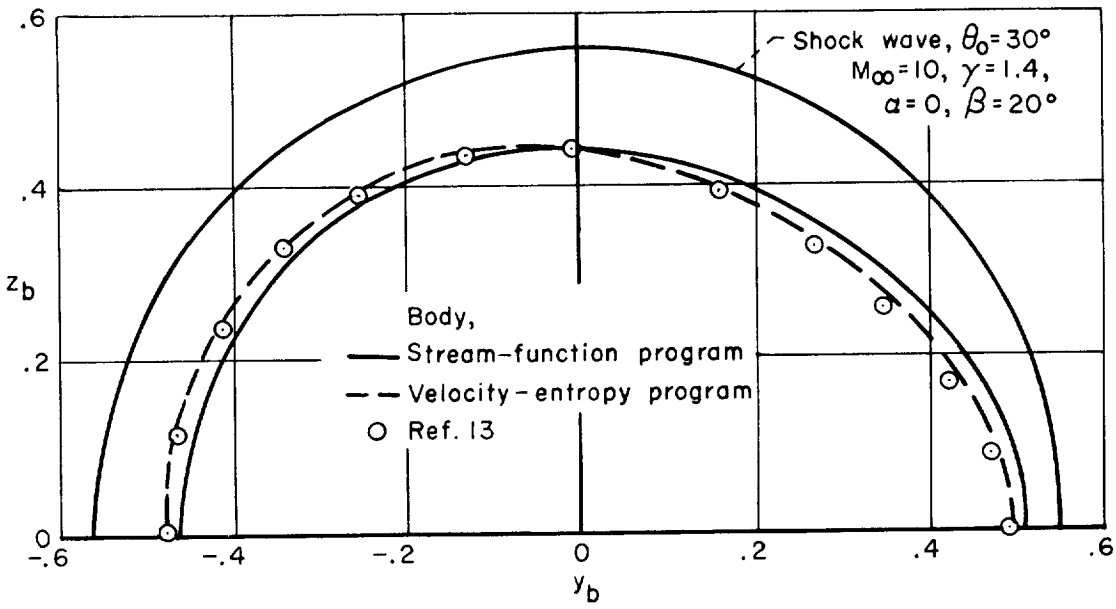

(a) Body and shock wave shapes

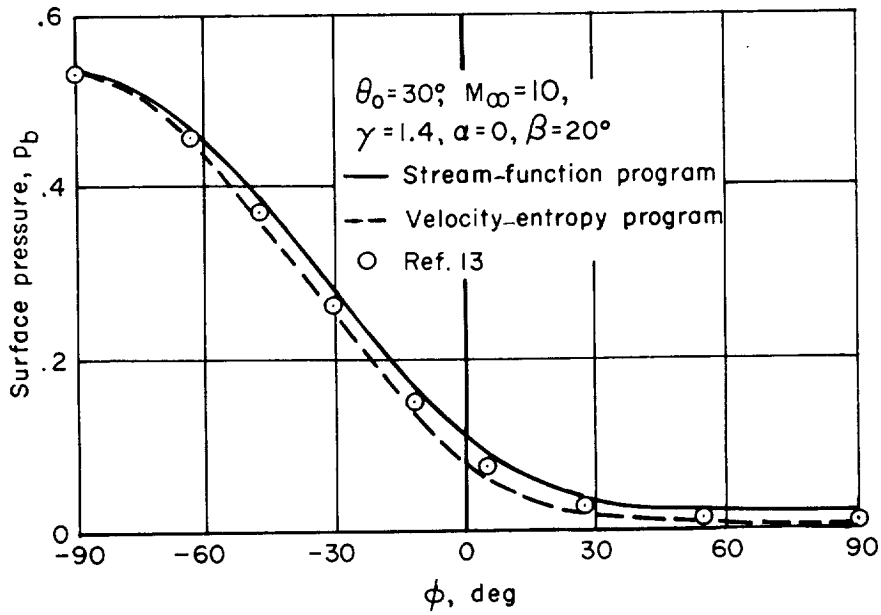

(b) Surface pressure

Figure 9.- Body and surface pressure for a circular conical shock wave at a finite angle of yaw.

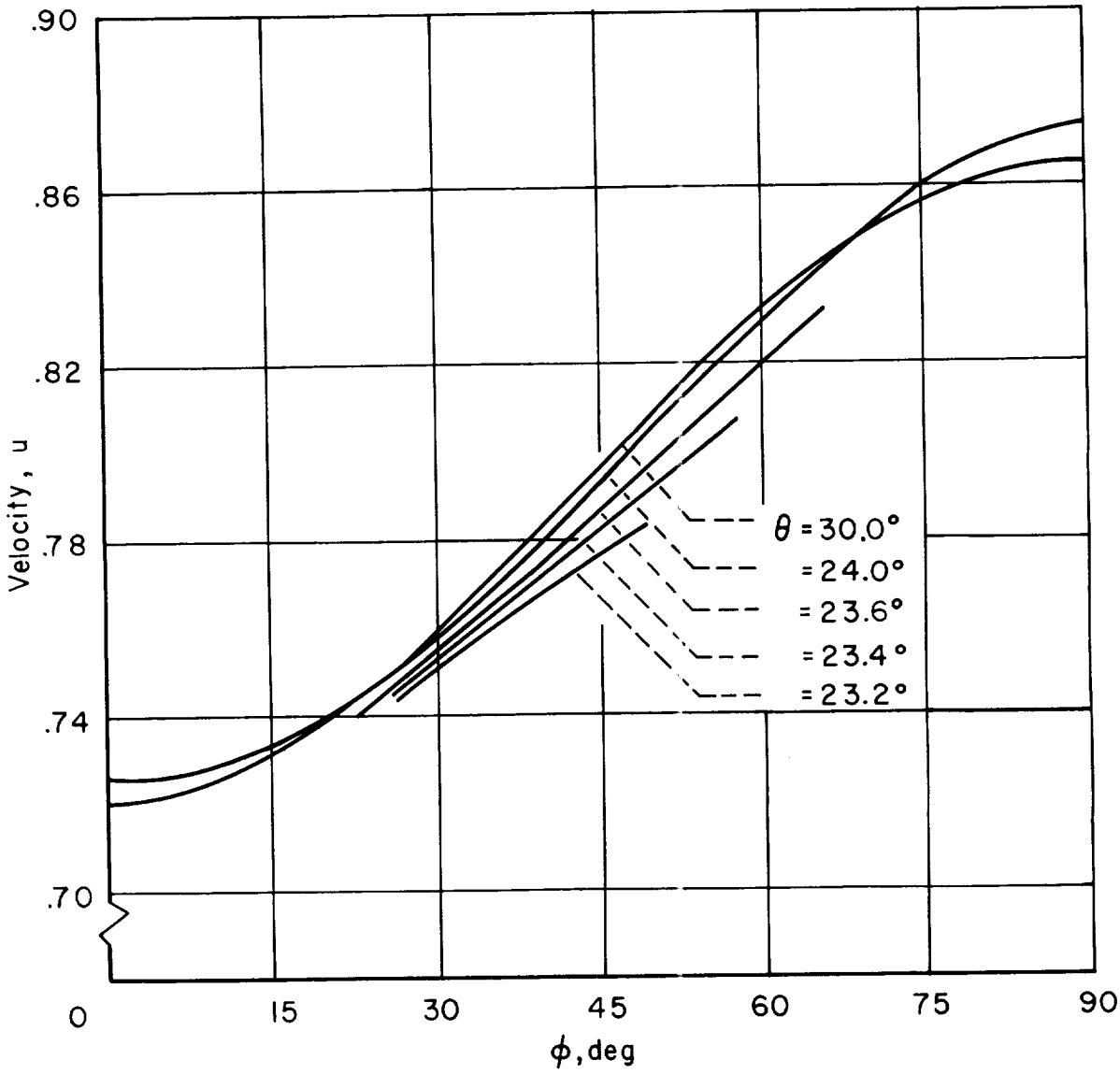

Figure 10.- The variation of the velocity component u in the flow field behind the shock for the case where $\theta_o = 30^o$, $M_\infty = 6$, $b_1/a_1 = 0.6$, $\gamma = 1.4$, $\alpha = \beta = 0$.

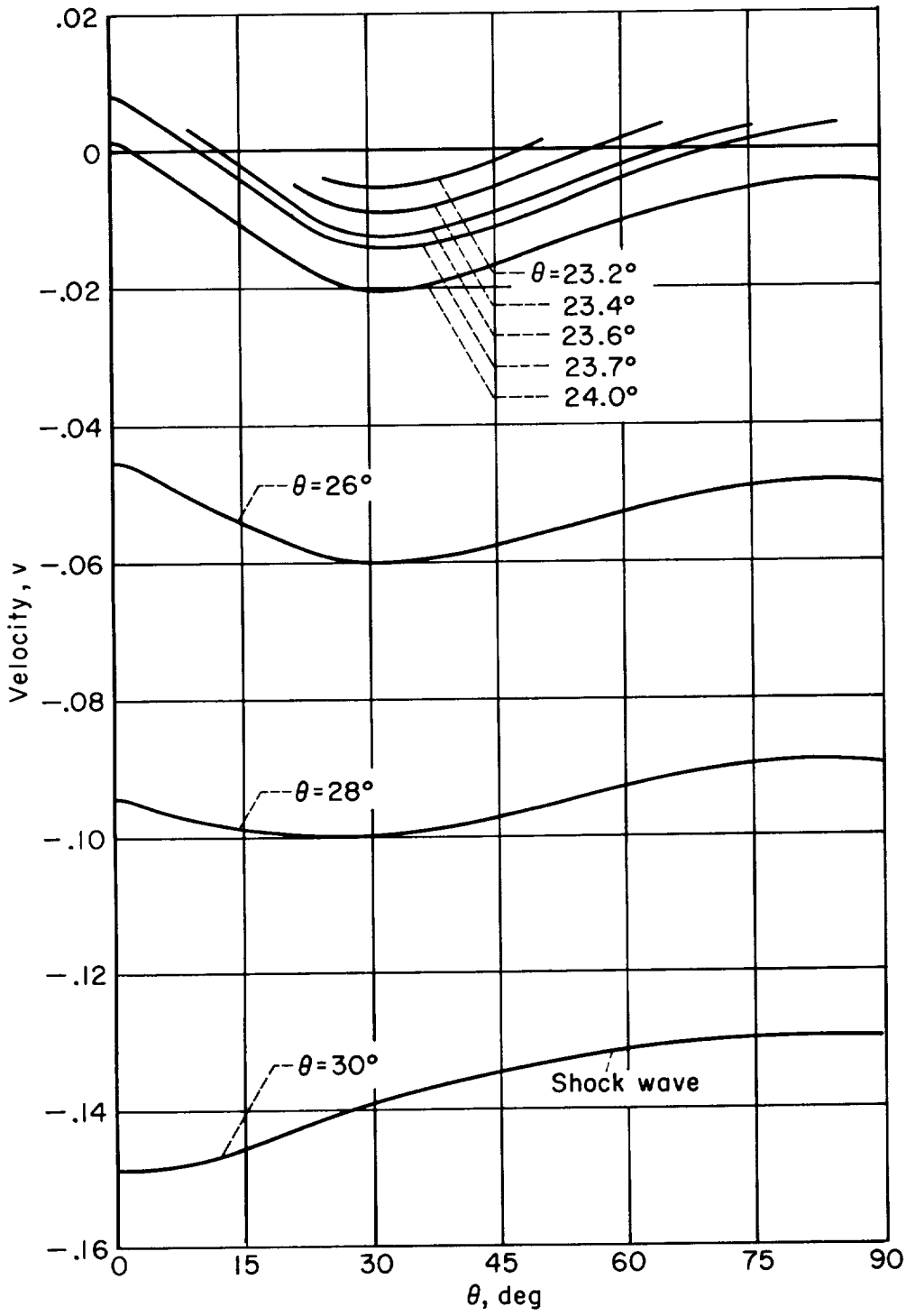

Figure 11.- The variation of the velocity component v in the flow field behind the shock for the case where $\theta_o = 30^o$, $M_\infty = 6$, $b_1/a_1 = 0.6$, $\gamma = 1.4$, $\alpha = \beta = 0$.

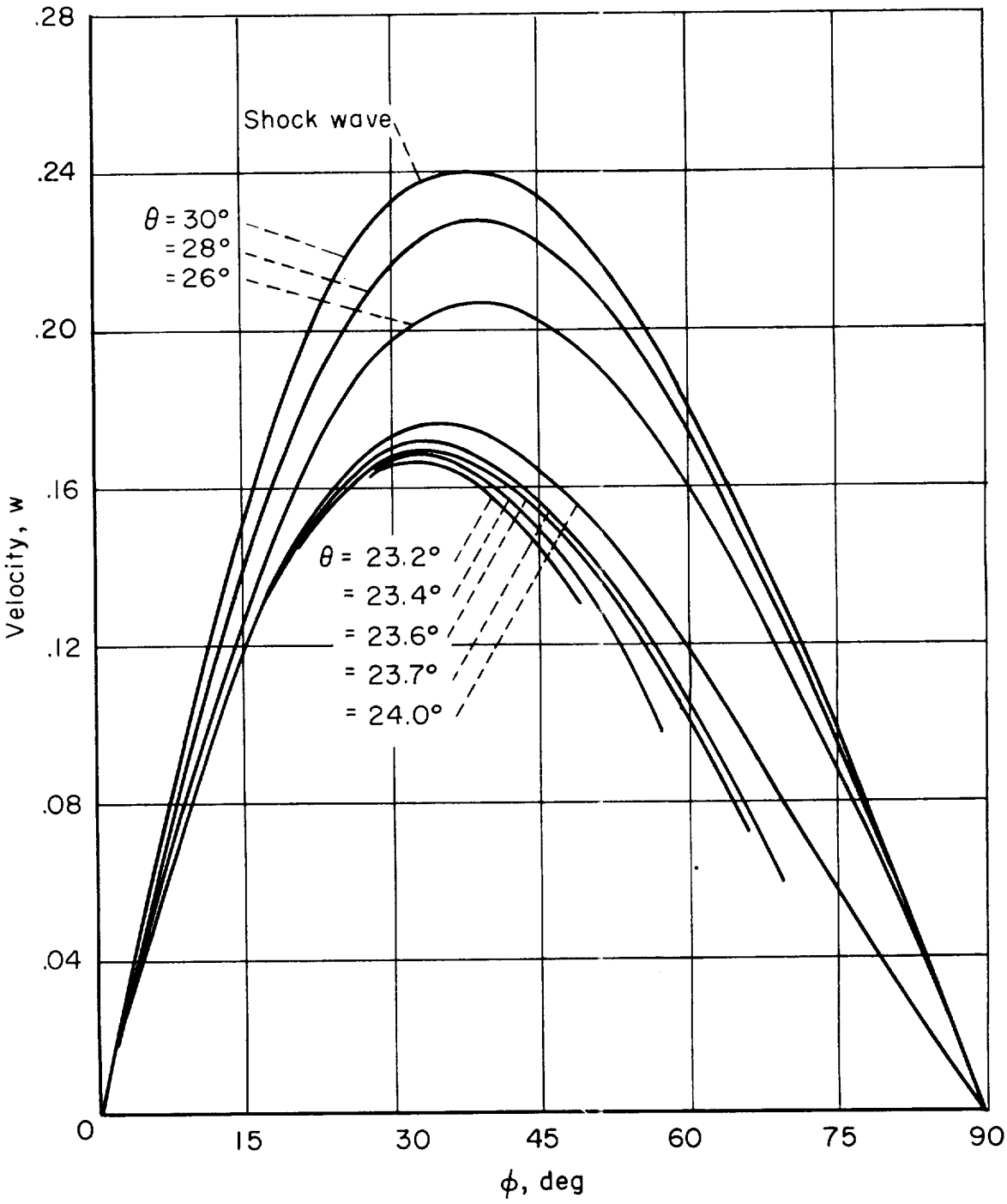

Figure 12.- The variation of the velocity component w in the flow field behind the shock for the case where $\theta_o = 30^o$, $M_\infty = 6$, $b_1/a_1 = 0.6$, $\gamma = 1.4$, $\alpha = \beta = 0$.

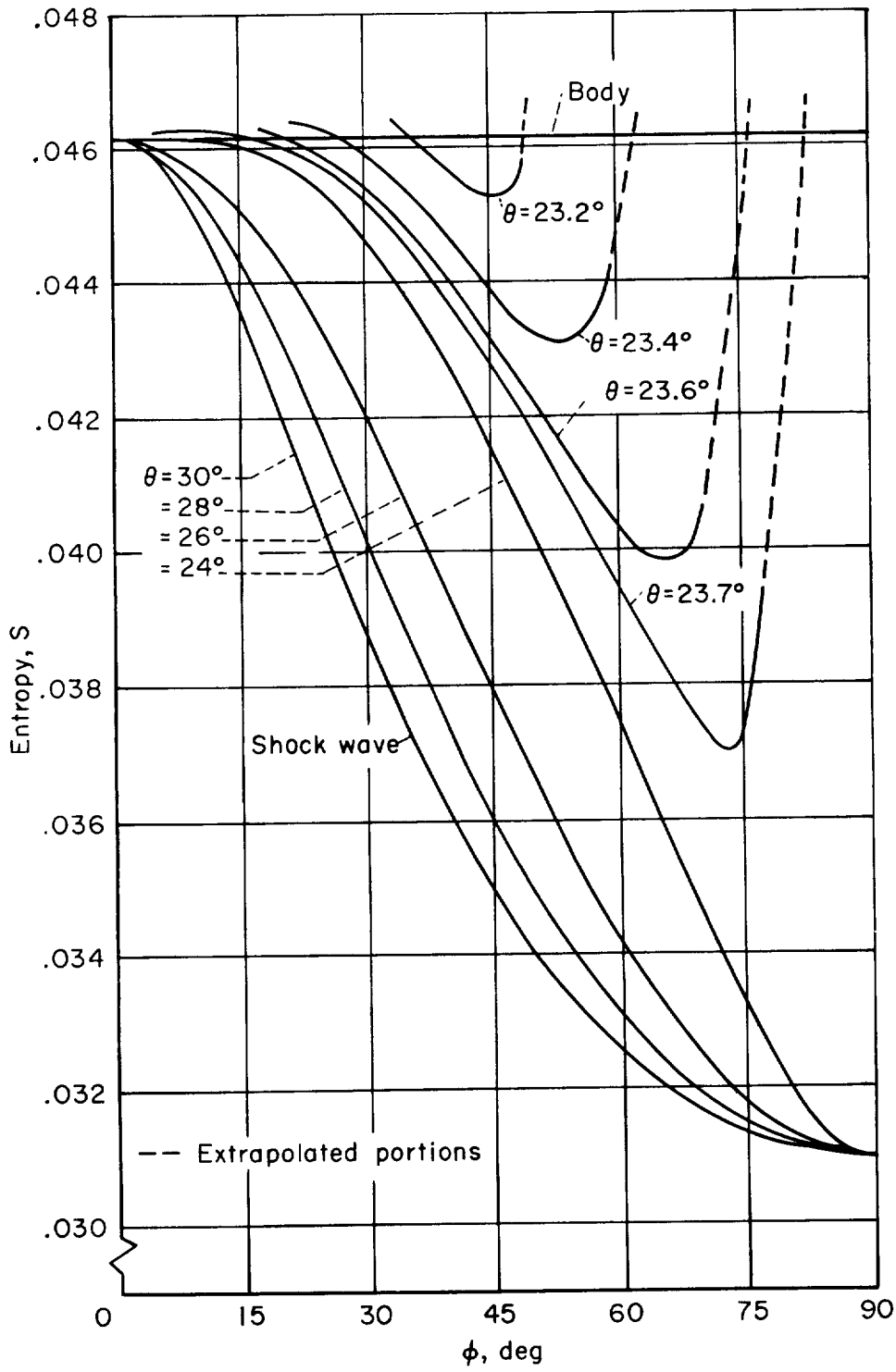

Figure 13.- The variation of entropy in the flow field behind the shock for the case where $\theta_o = 30^o$, $M_\infty = 6$, $b_1/a_1 = 0.6$, $\gamma = 1.4$, $\alpha = \beta = 0$.

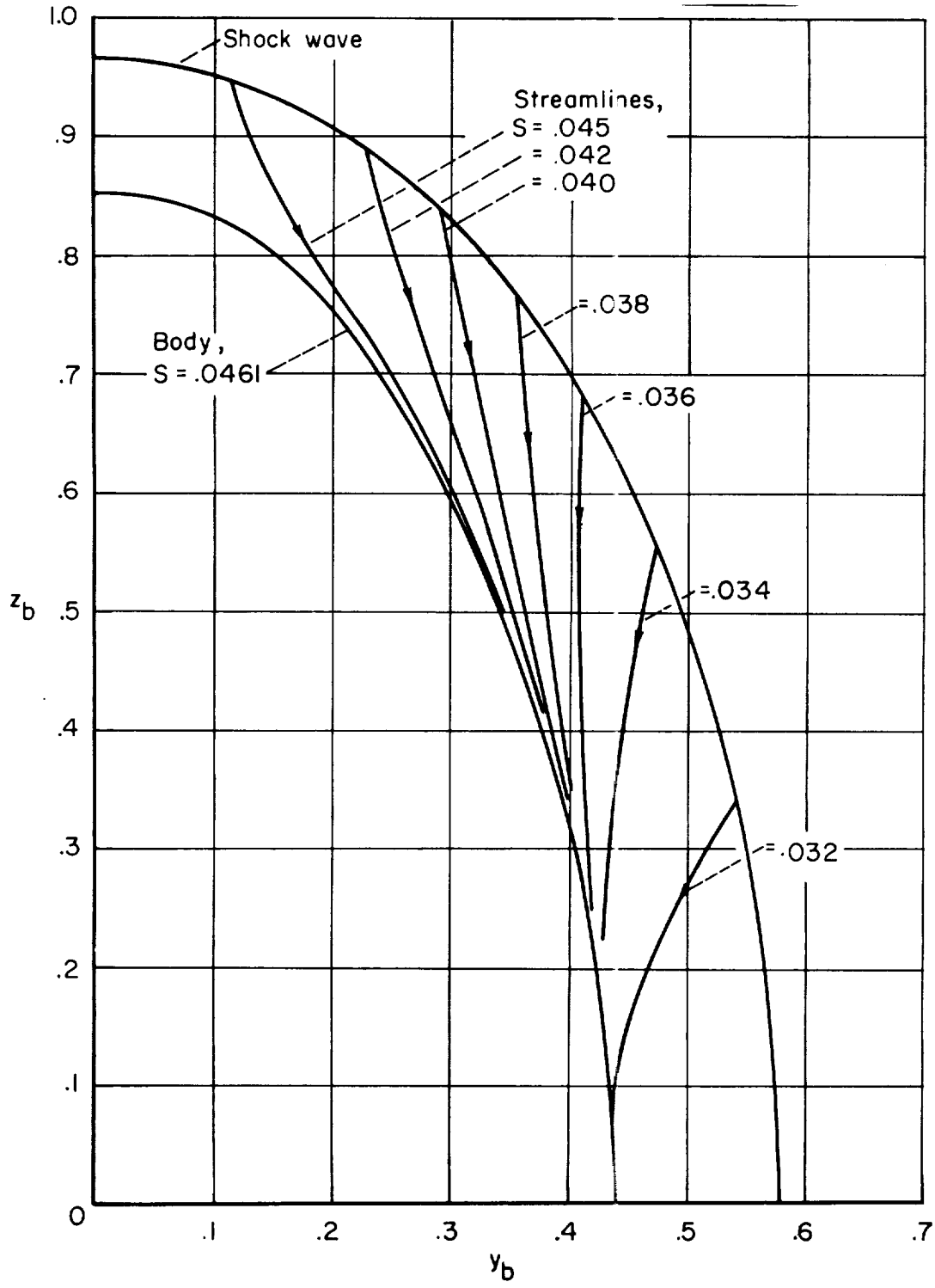

Figure 14.- Streamlines in the crossflow between shock and body for the case where $\theta_o = 30^o$, $M_\infty = 6$, $b_1/a_1 = 0.6$, $\gamma = 1.4$, $\alpha = \beta = 0$.

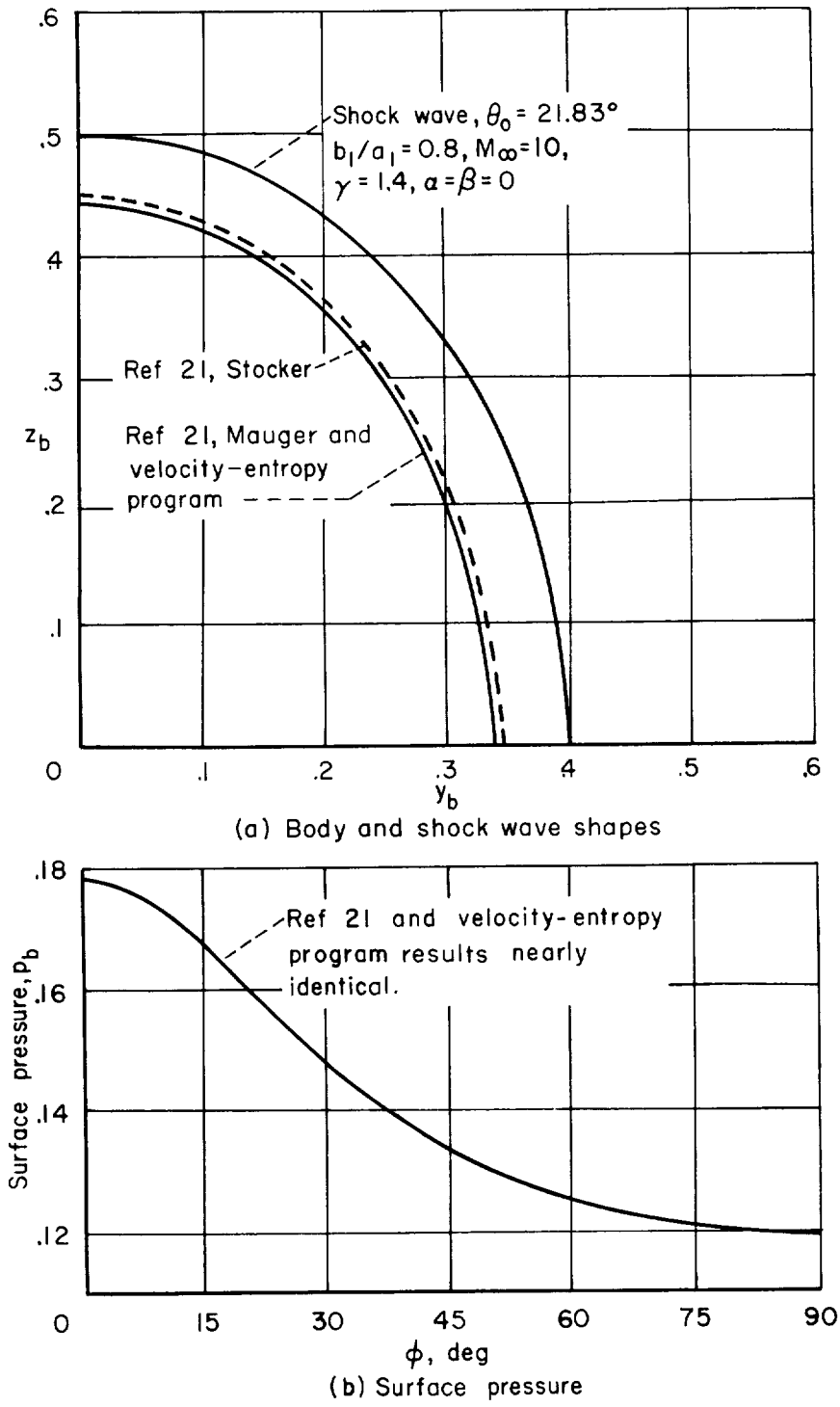

Figure 15.- Comparison of body shape and surface pressure for an elliptic conical shock wave as calculated by the velocity-entropy program and the methods of Stocker and Mauger.

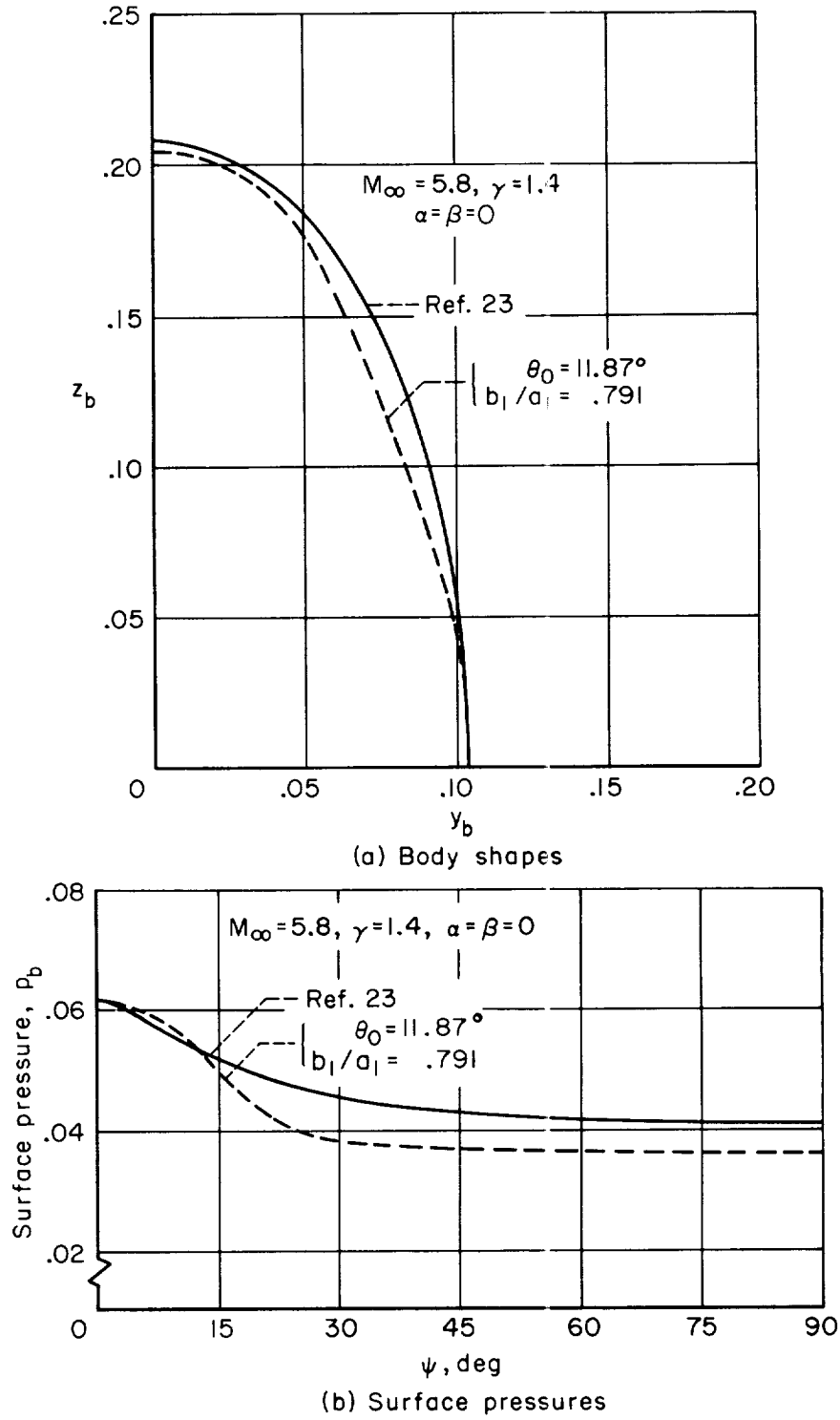

Figure 16.- Comparisons of calculations with experiments on an elliptic cone of unit length having semiaxes of lengths 0.104 and 0.208.

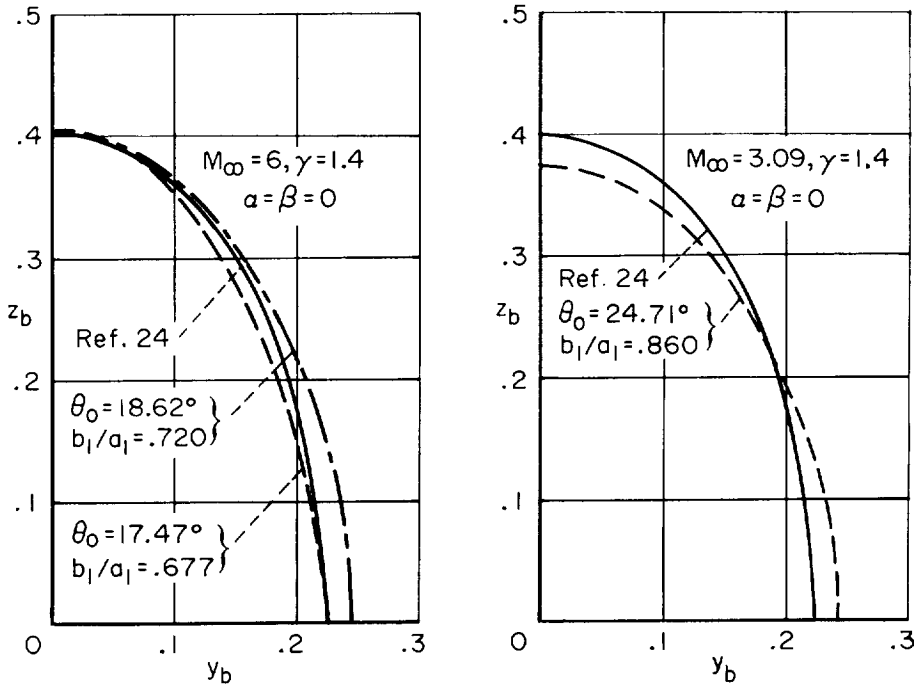

(a) Body shapes

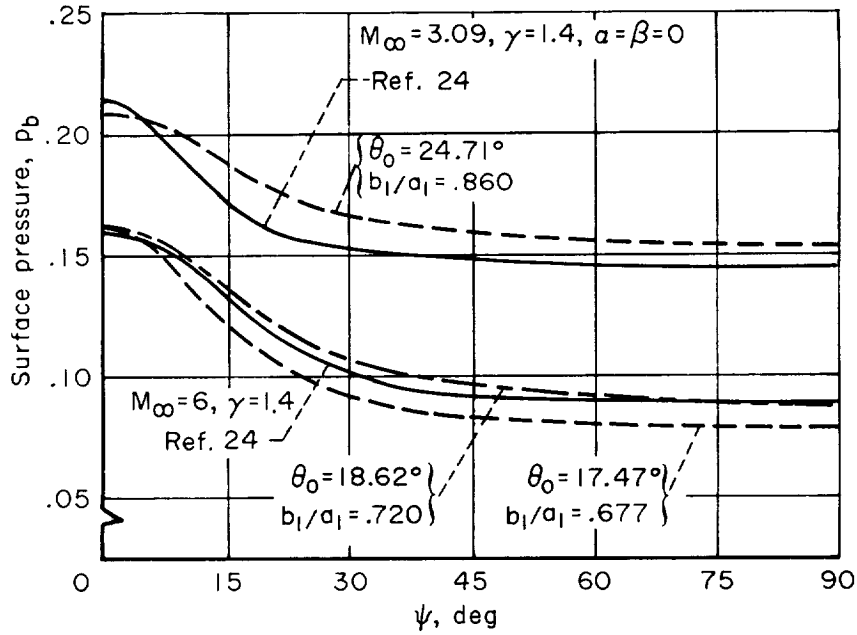

(b) Surface pressures

Figure 17.- Comparison of calculations with experiments on an elliptic cone of unit length having semiaxes of lengths 0.225 and 0.402.

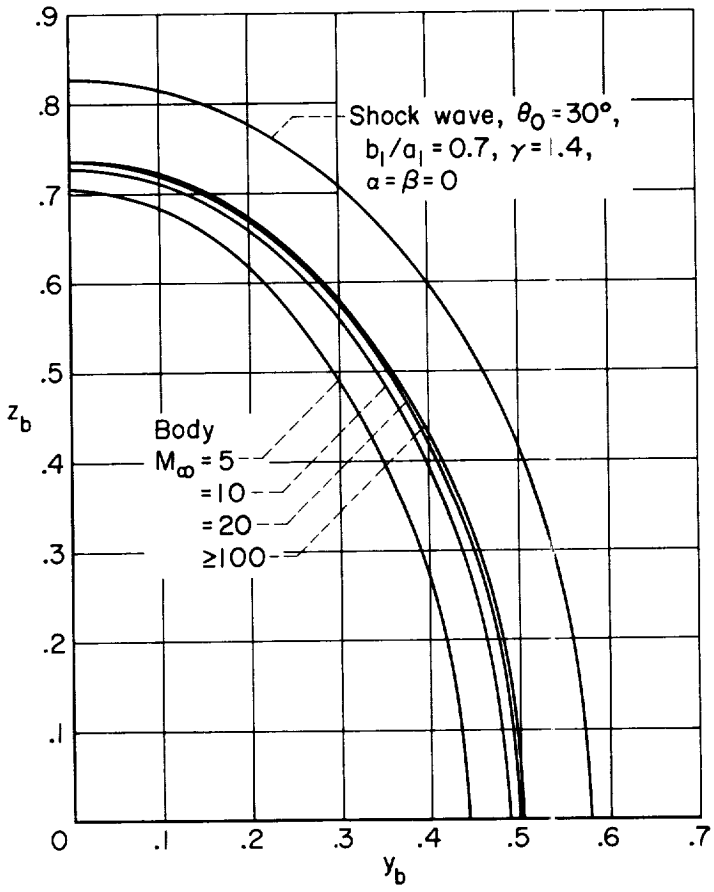

(a) Body and shock wave shapes

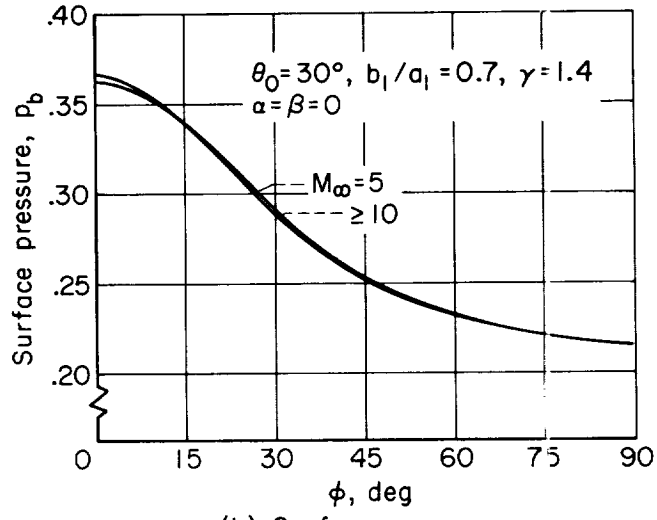

(b) Surface pressures

Figure 20.- The effect of Mach number variation on body shape and surface pressure; $b_1/a_1 = 0.7$ series.

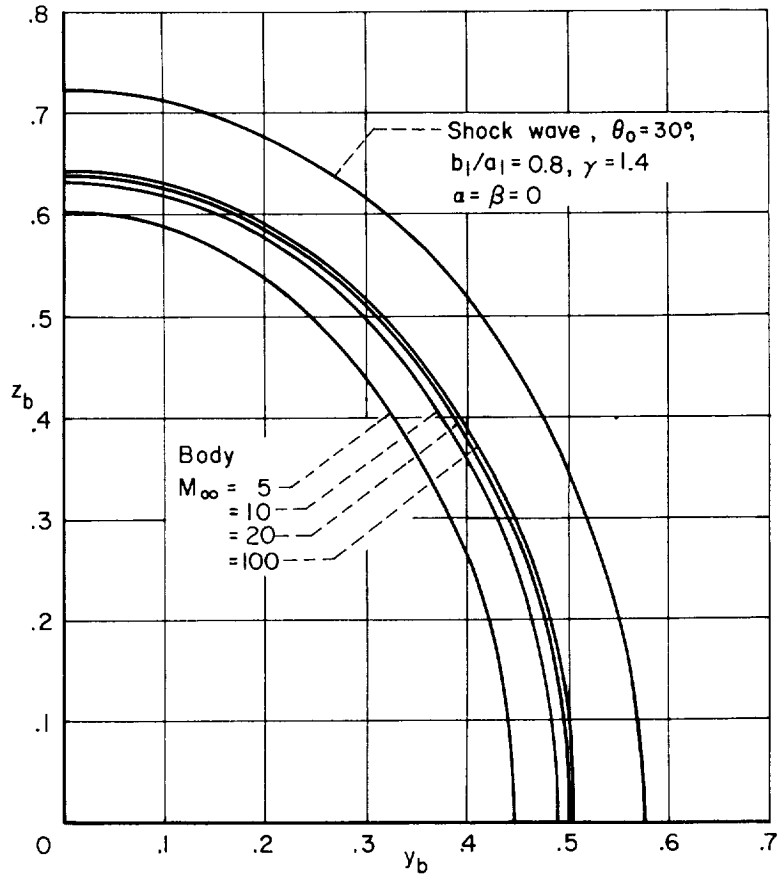

(a) Body and shock wave shapes

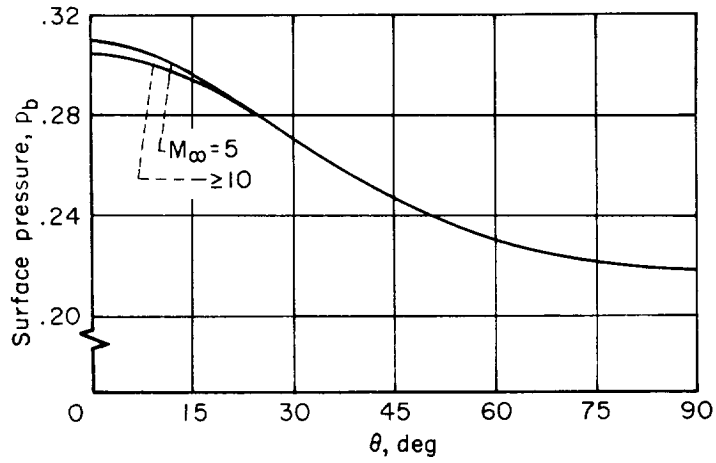

(b) Surface pressure

Figure 21.- The effect of Mach number variation on body shape and surface pressure; $b_1/a_1 = 0.8$ series.

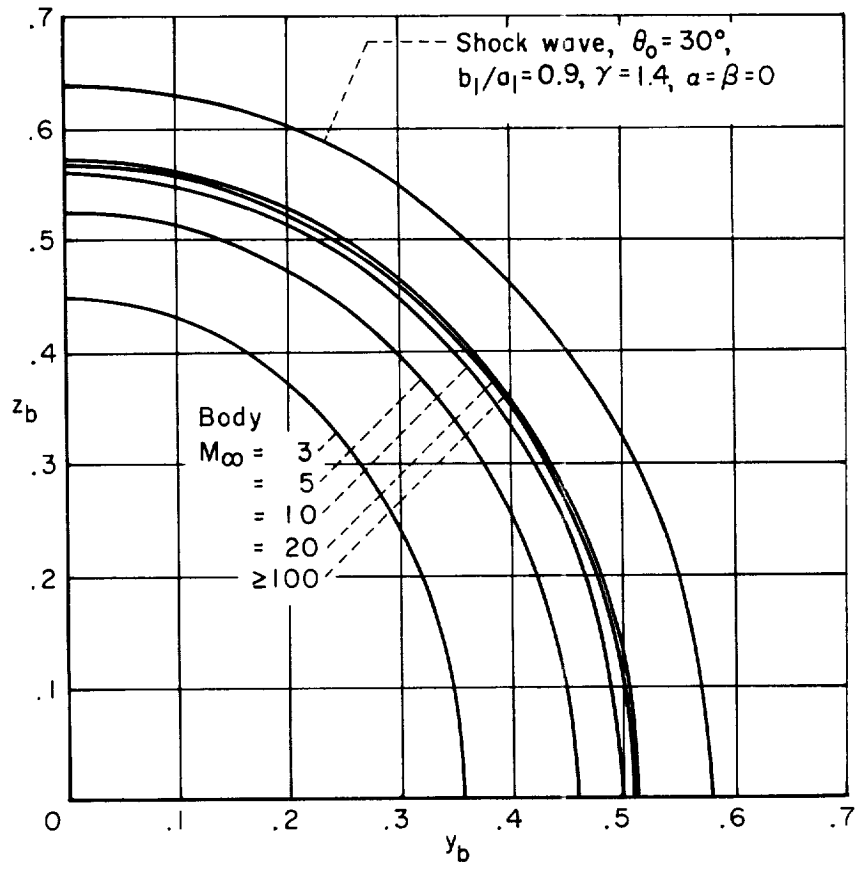

(a) Body and shock wave shapes

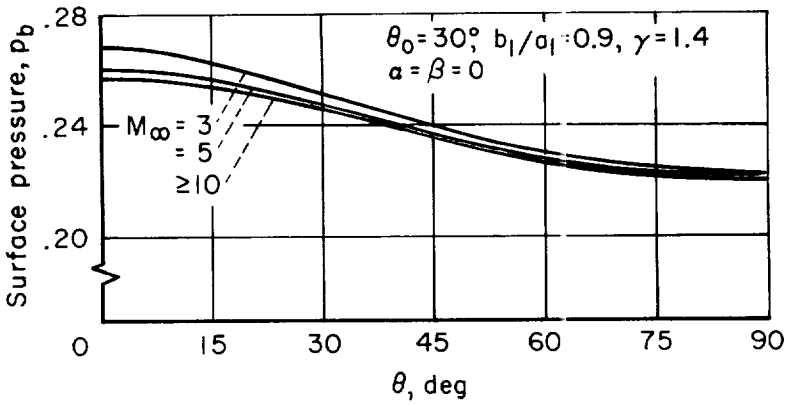

(b) Surface pressure

Figure 22.- The effect of Mach number variation on body shape and surface pressure; $b_1/a_1 = 0.9$ series.

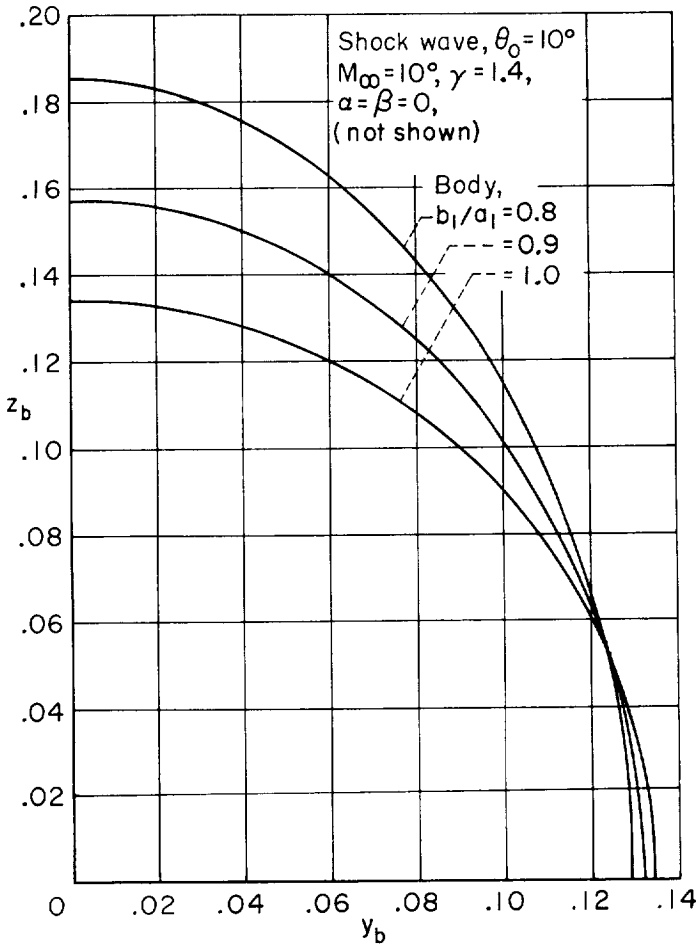

(a) Body shapes

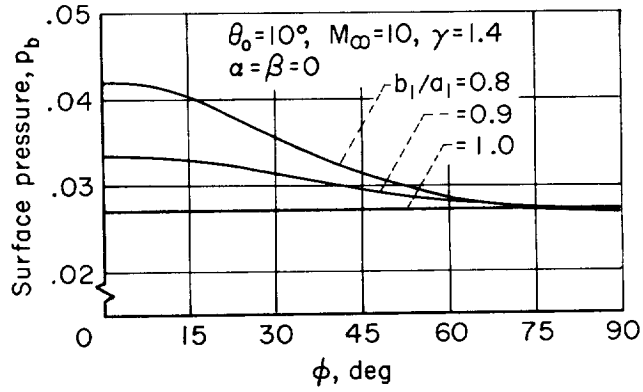

(b) Surface pressure

Figure 23.- The effect of the variation of b_1/a_1 on body shape and surface pressure; $\theta_0 = 10^\circ$ series.

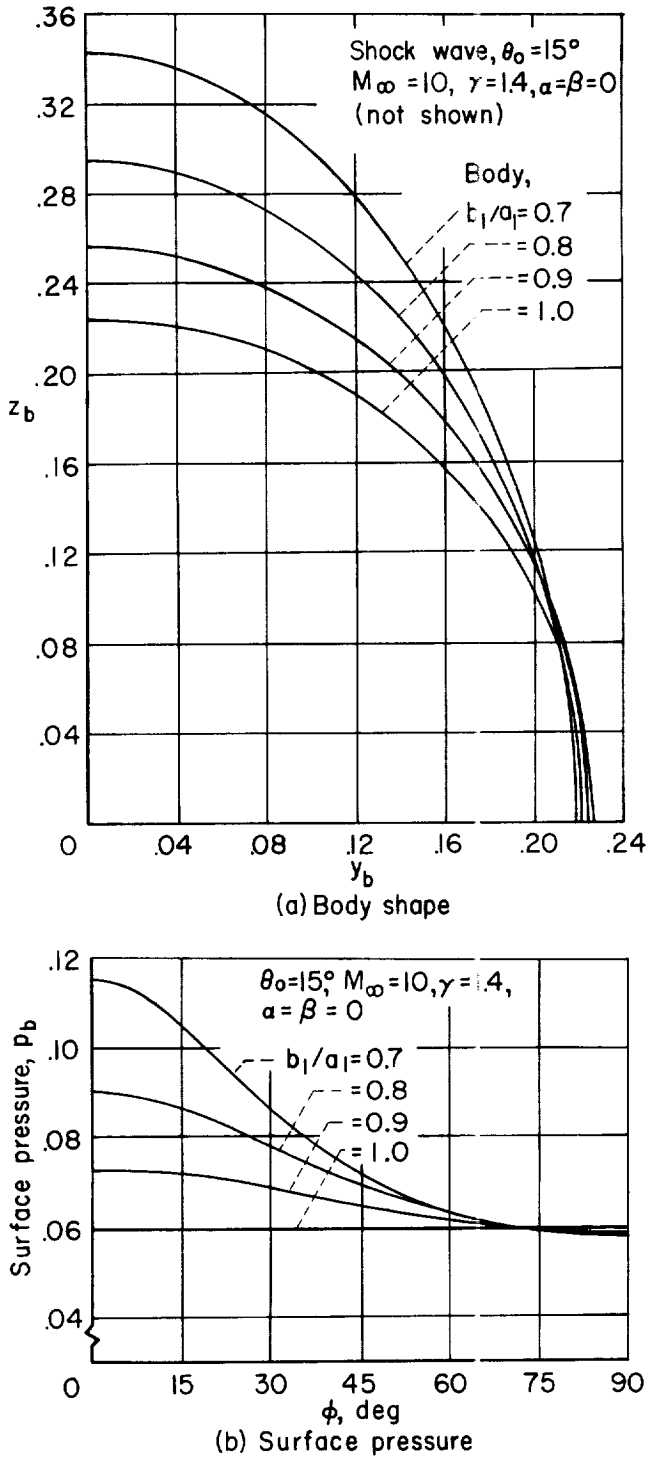

Figure 24.- The effect of the variation of b_1/a_1 on body shape and surface pressure; θ_o = 15° series.

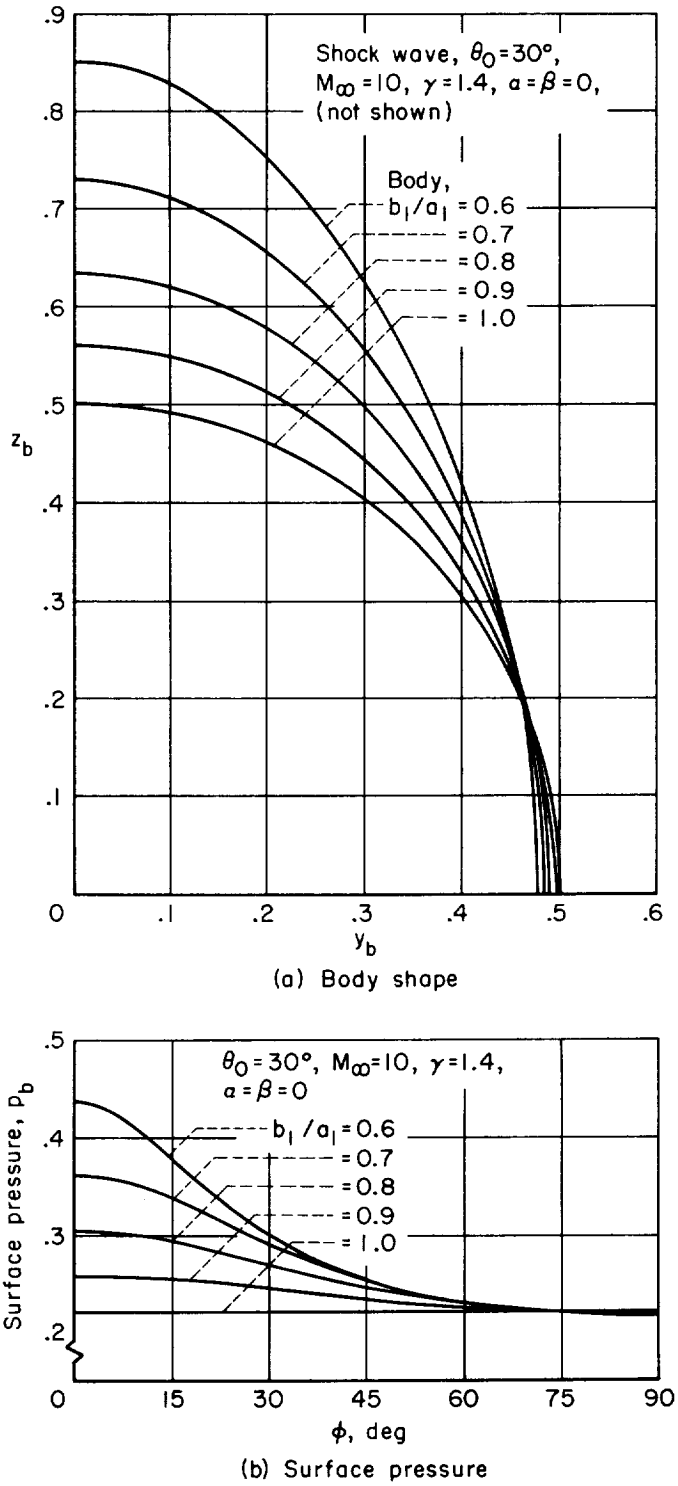

Figure 25.- The effect of the variation of b_1/a_1 on body shape and surface pressure; $\theta_0 = 30^\circ$ series.

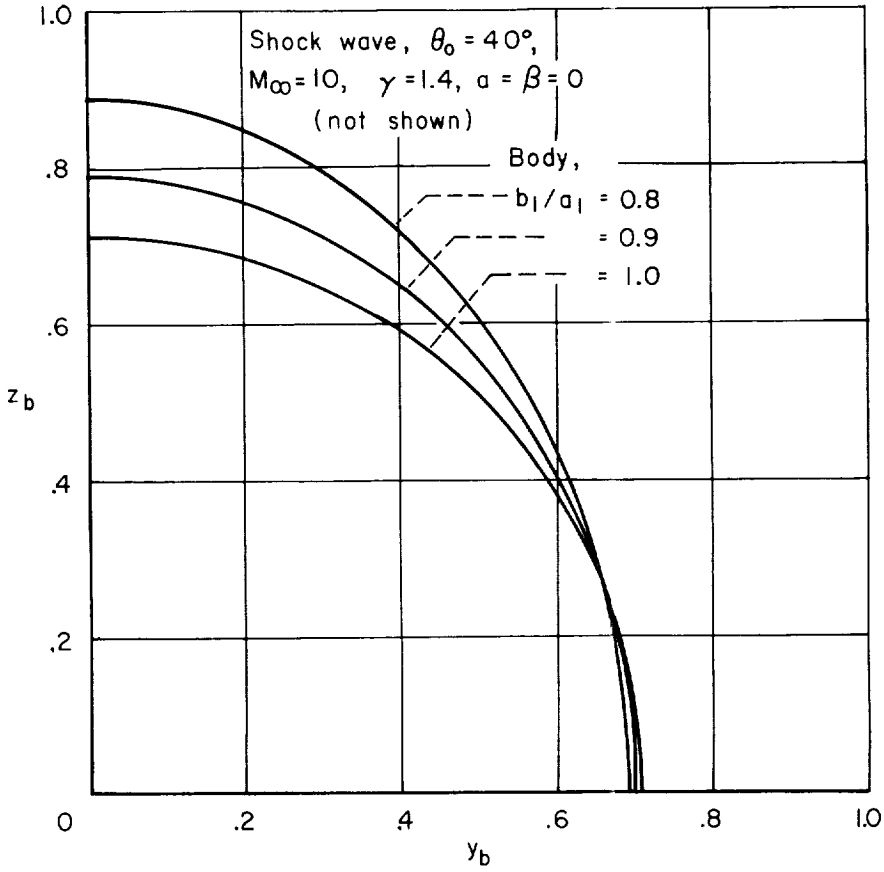

(a)Body shapes

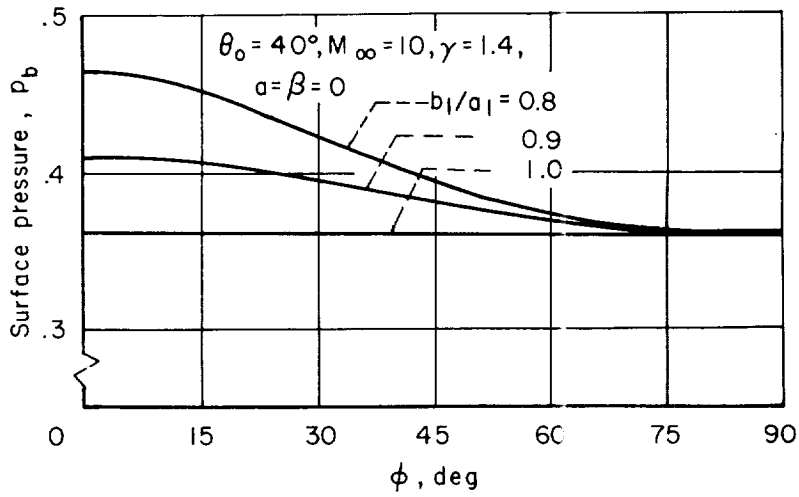

(b) Surface pressures

Figure 26.- The effect of the variation of b_1/a_1 on body shape and surface pressure; $\theta_o = 40°$ series.

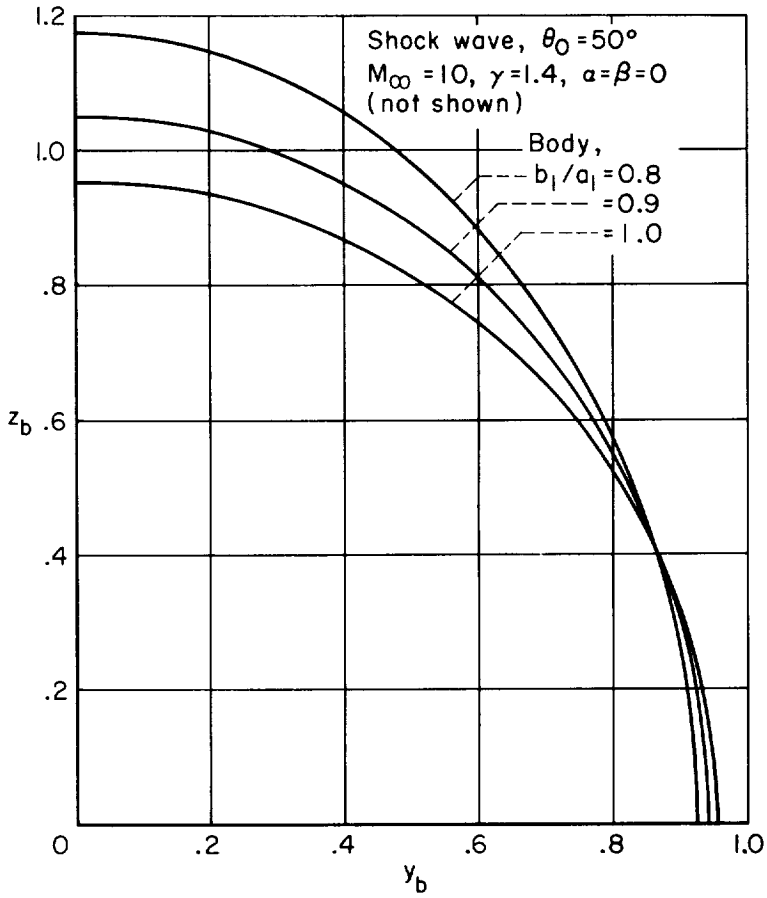

(a) Body shape

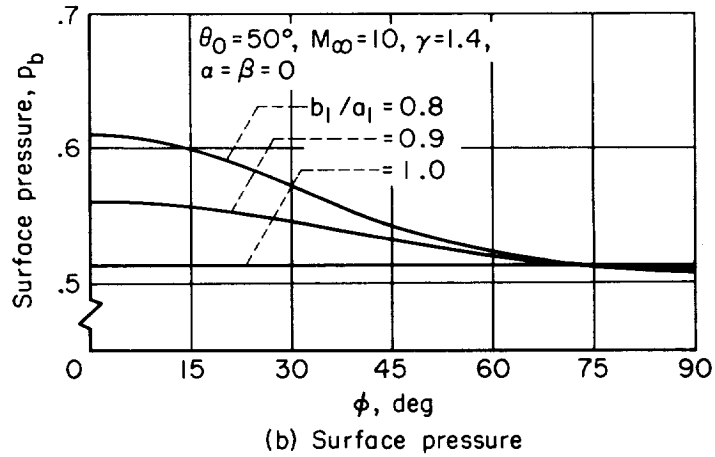

(b) Surface pressure

Figure 27.- The effect of the variation of b_1/a_1 on body shape and surface pressure; $\theta_0 = 50°$ series.

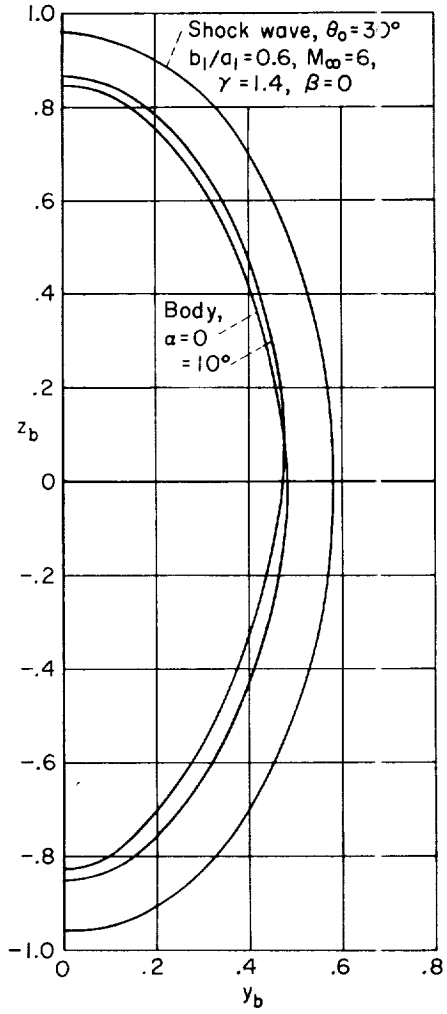

(a) Body shapes

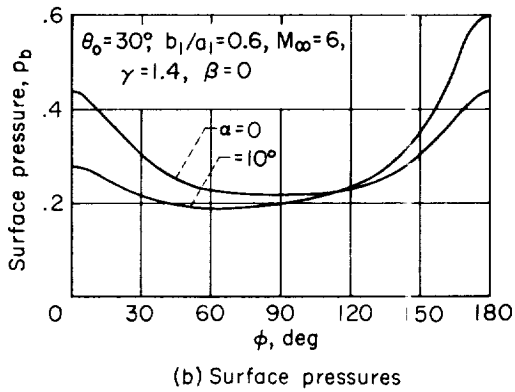

(b) Surface pressures

Figure 28.- The effect of α on body shape and surface pressure; an elliptic conical shock wave.

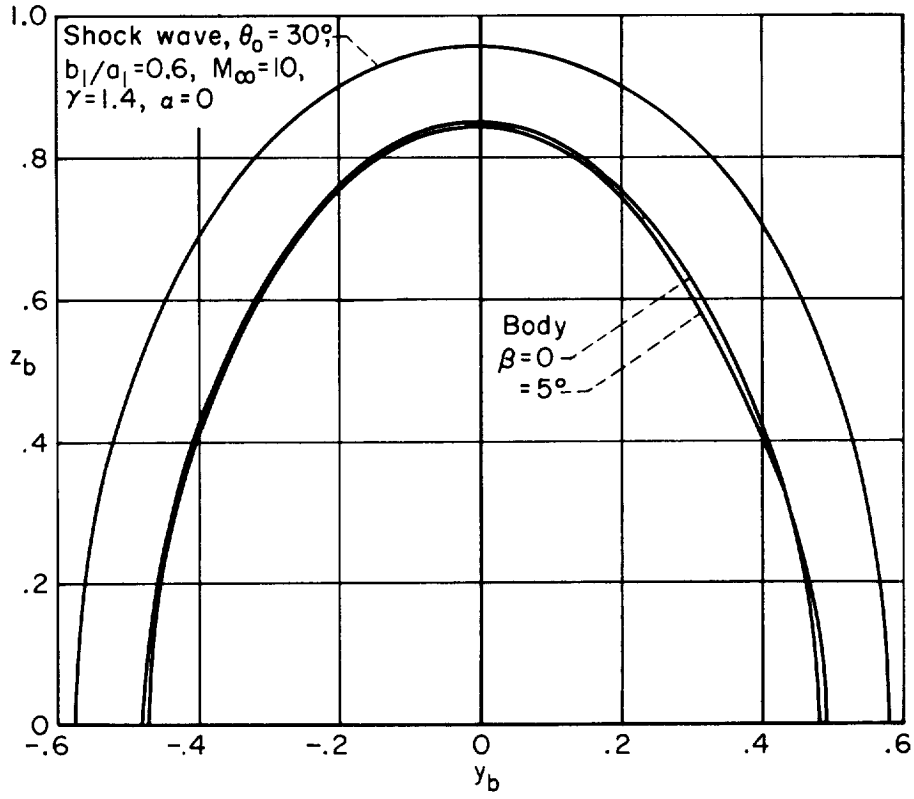

(a) Body and shock wave shapes

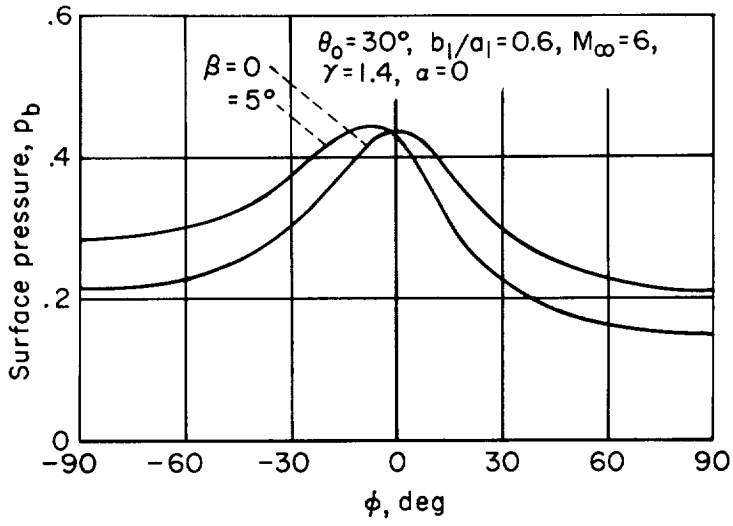

(b) Surface pressures

Figure 29.- The effect of β on body shape and surface pressure; an elliptic conical shock wave.

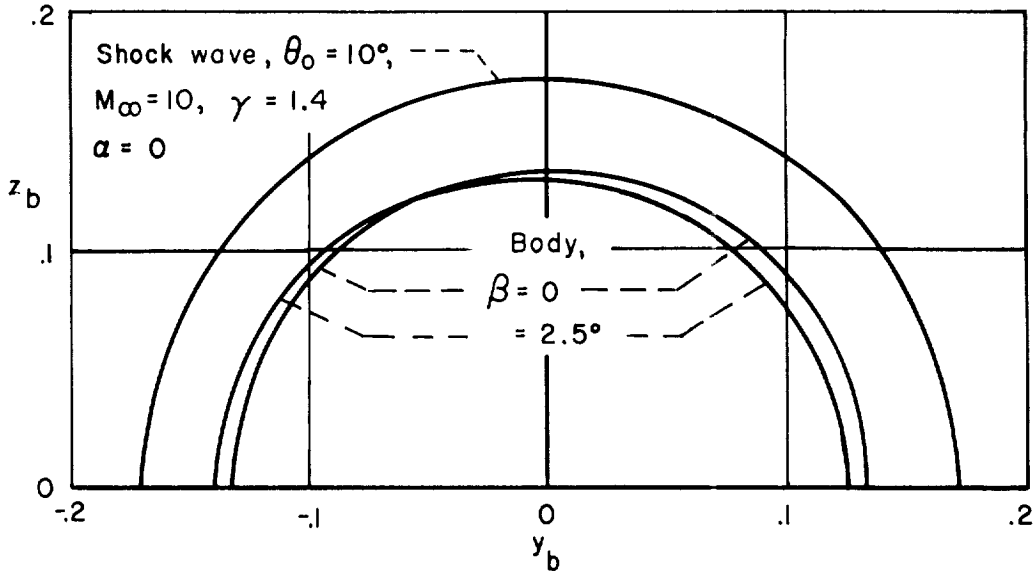

(a) Body and shock wave shapes

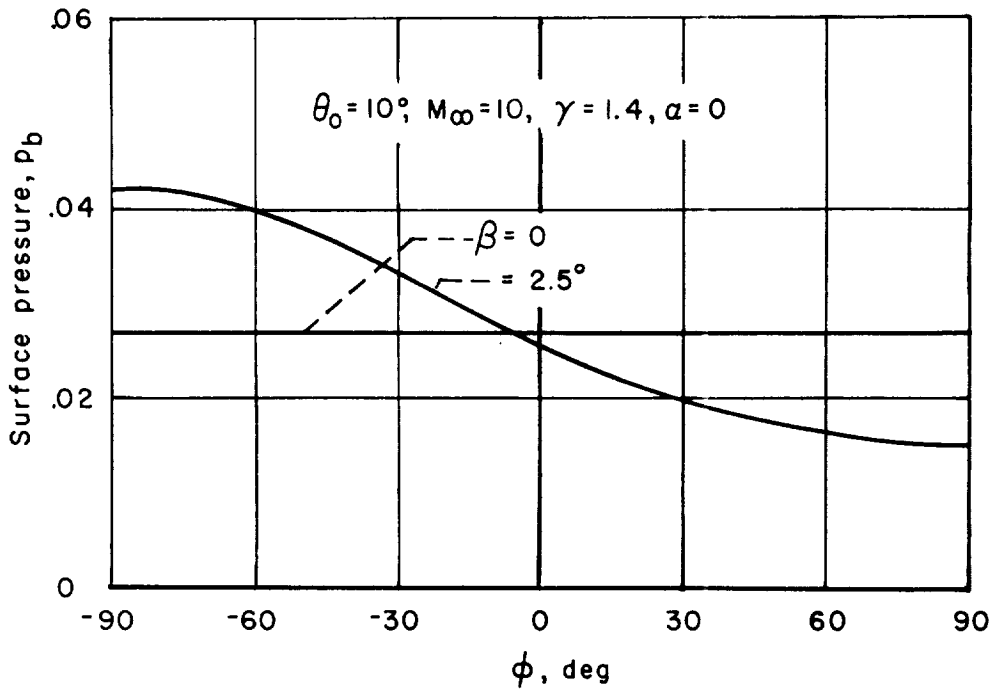

(b) Surface pressures

Figure 30.- The effect of β on body shape and surface pressure; circular conical shock with $\theta_0 = 10^\circ$.

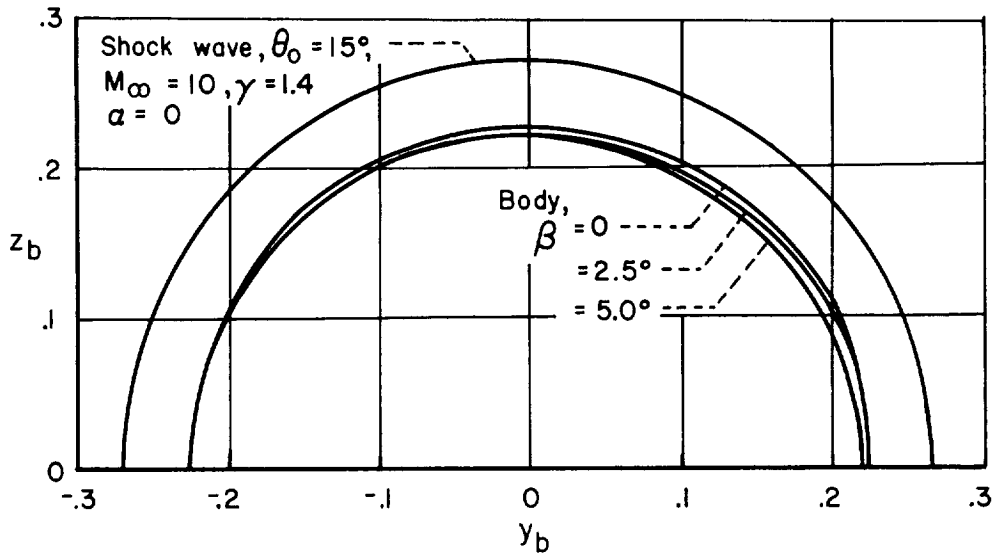

(a) Body and shock wave shapes

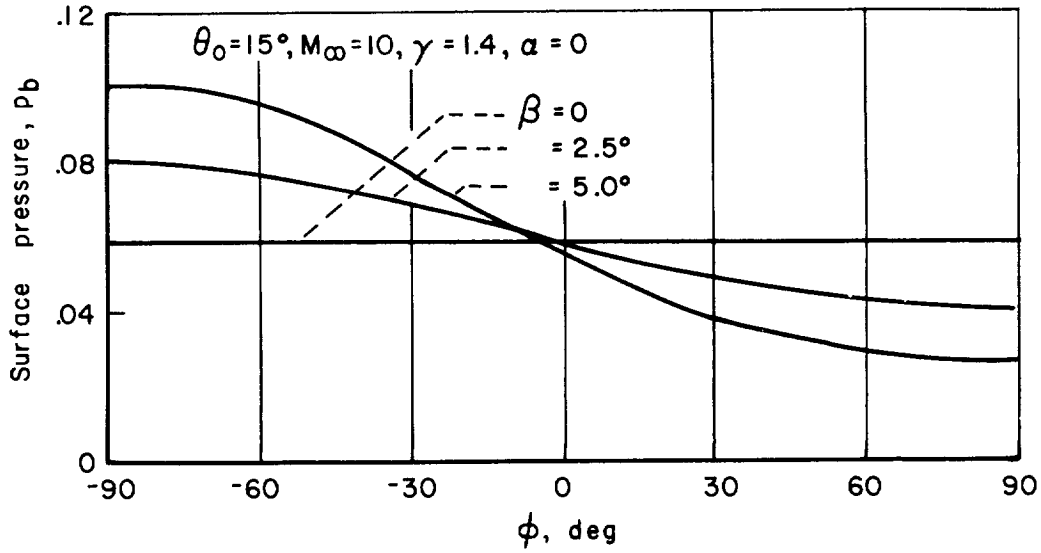

(b) Surface pressures

Figure 31.- The effect of β on body shape and surface pressure; circular conical shock with $\theta_0 = 15^\circ$.

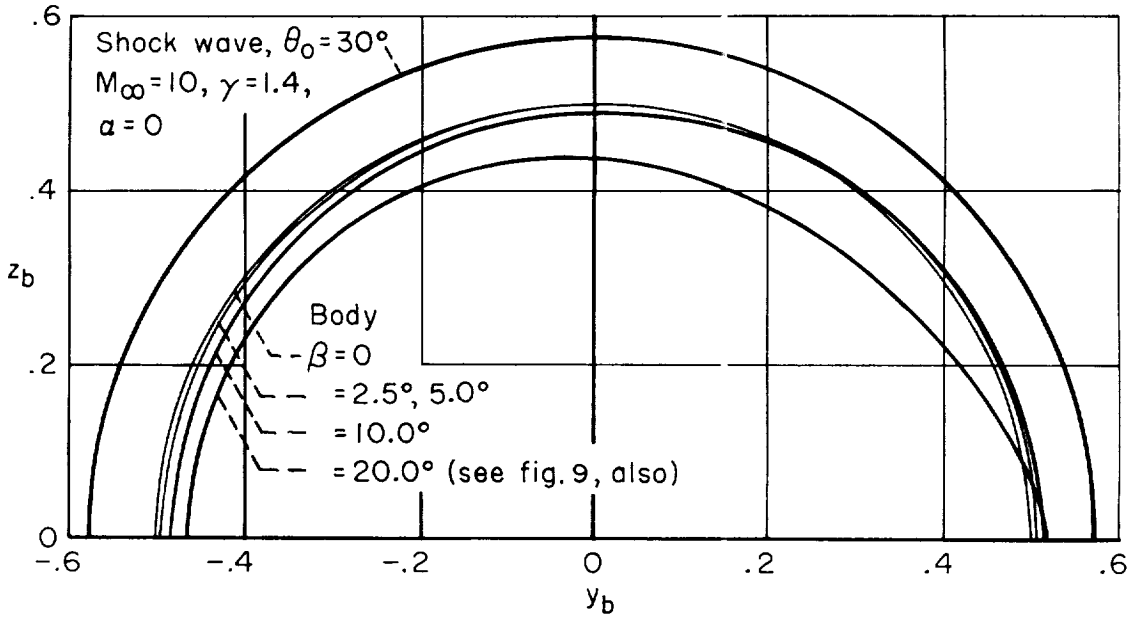

(a) Body and shock wave shapes

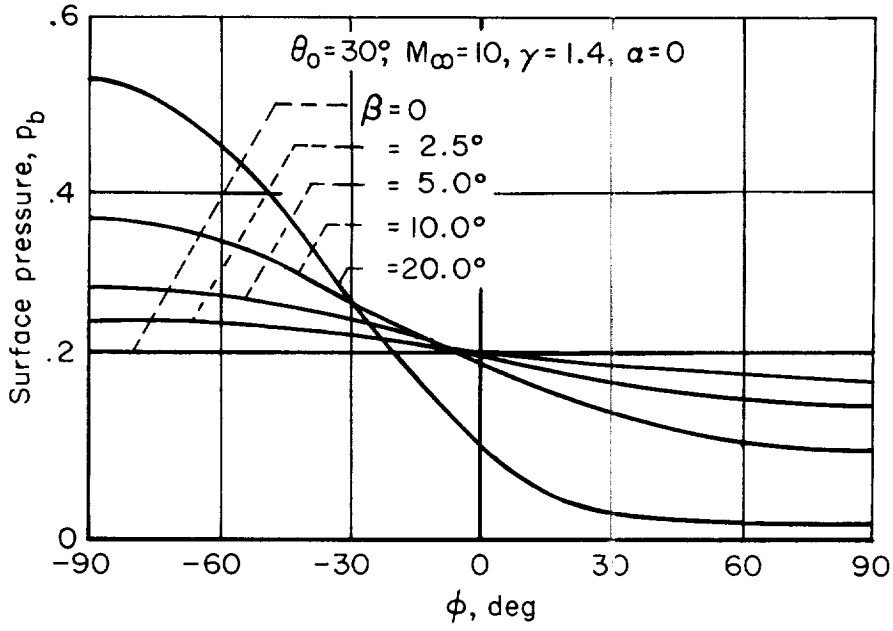

(b) Surface pressures

Figure 32.- The effect of β on body shape and surface pressure; circular conical shock with $\vartheta_0 = 30^\circ$.

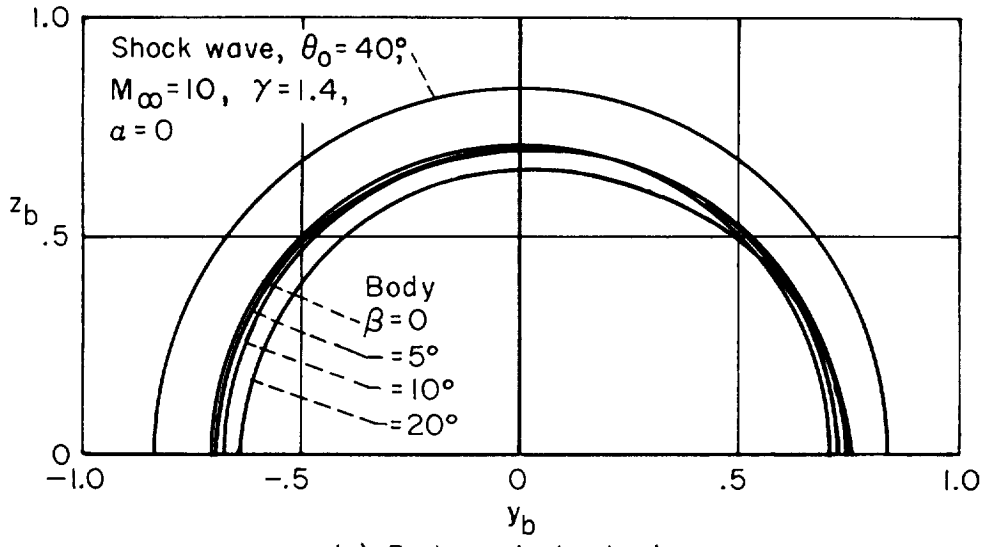

(a) Body and shock shapes

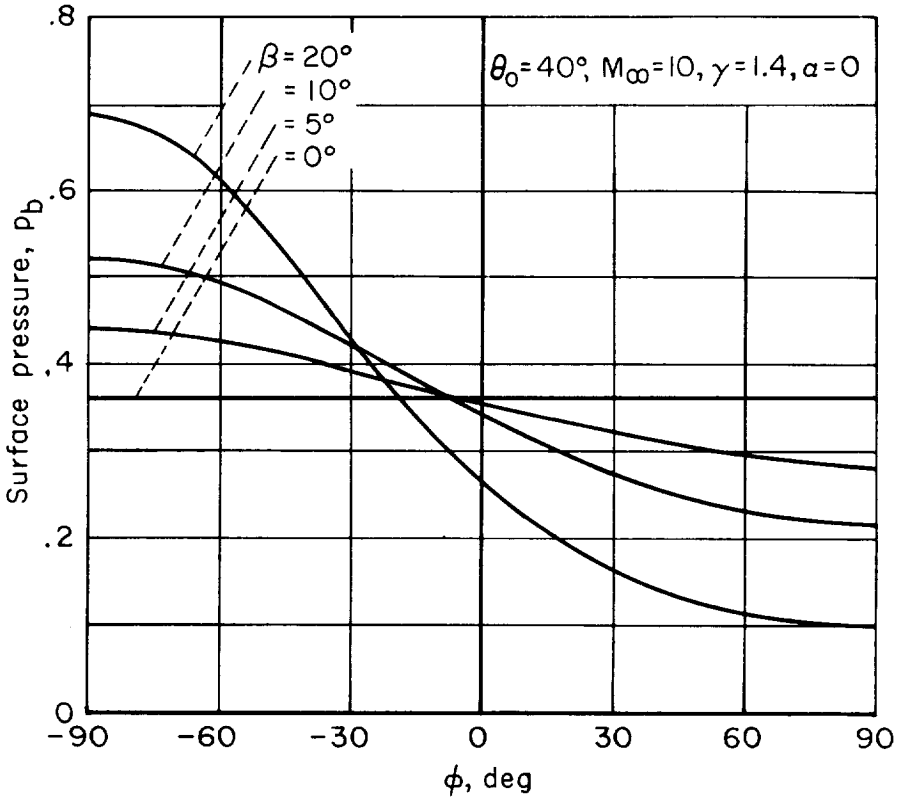

(b) Surface pressures

Figure 33.- The effect of β on body shape and surface pressure; circular conical shock with $\theta_o = 40°$.

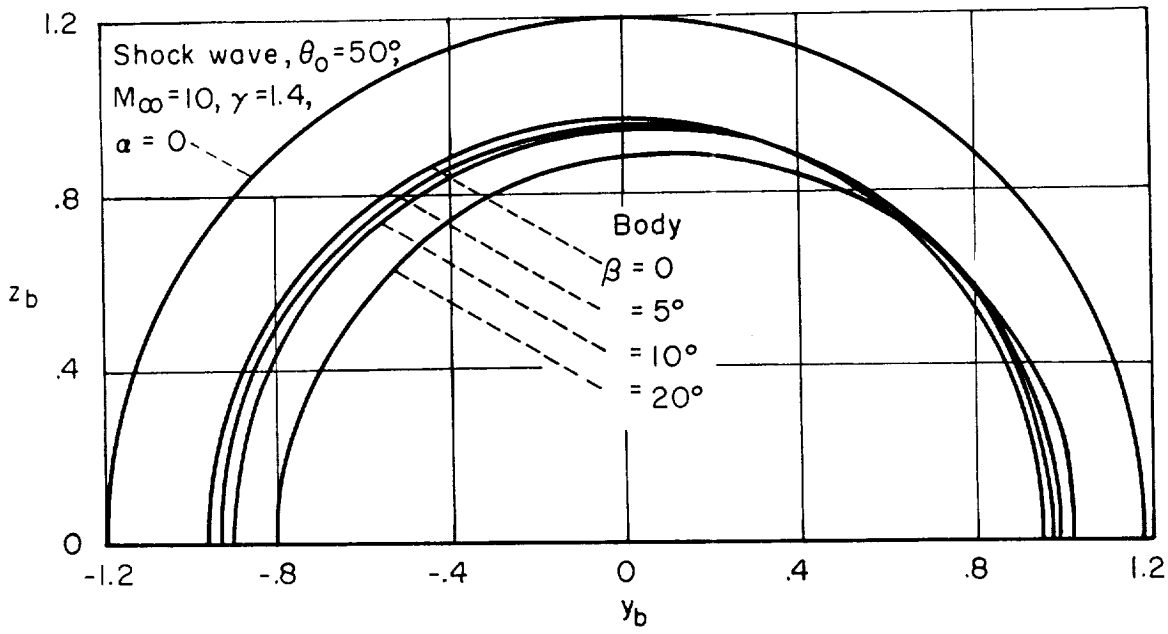

(a) Body and shock wave shapes

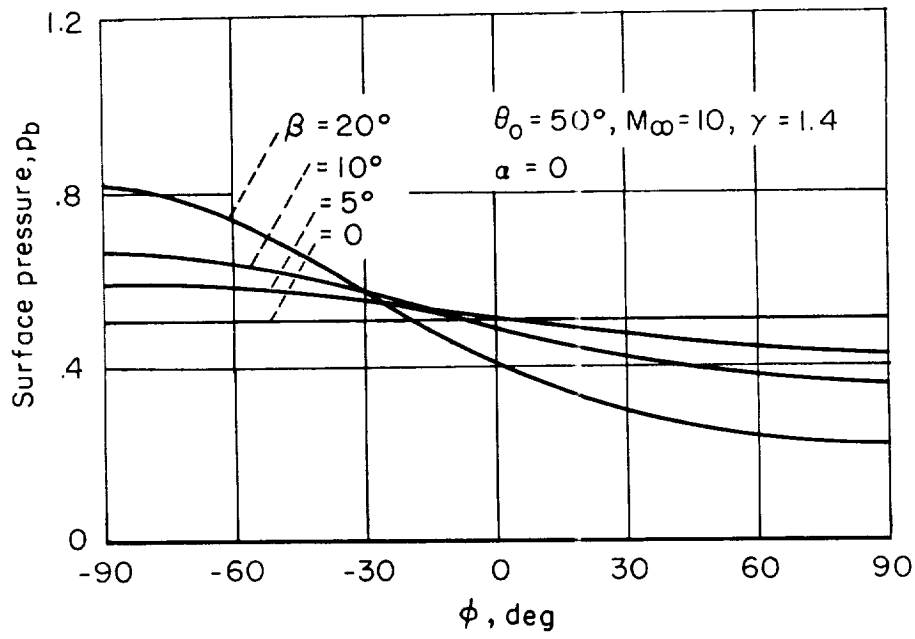

(b) Surface pressures

Figure 34.- The effect of β on body shape and surface pressure; circular conical shock with $\theta_0 = 50°$.